International Journal of Multiphase Flow 36 (2010) 643–660

Contents lists available at ScienceDirect

International Journal of Multiphase Flow

journal homepage: www.elsevier.com/locate/ijmulflow

Modeling and simulation of severe slugging in air–water pipeline–riser systems

J.L. Baliño [a,*], K.P. Burr [b], R.H. Nemoto [a]

[a] Departamento de Engenharia Mecânica, Escola Politécnica, Universidade de São Paulo, Av. Prof. Mello Moraes, 2231, CEP 05508-900, Cidade Universitária, São Paulo, SP, Brazil
[b] Centro de Engenharia, Modelagem e Ciências Sociais Aplicadas, Universidade Federal do ABC, Rua Santa Adélia 166, CEP 09210-170, Santo André, SP, Brazil

ARTICLE INFO

Article history:
Received 26 October 2009
Received in revised form 30 March 2010
Accepted 6 April 2010
Available online 18 April 2010

Keywords:
Severe slugging
Pipeline–riser system
Stability
Air–water flow
Petroleum production technology

ABSTRACT

A mathematical model, numerical simulations and stability and flow regime maps corresponding to severe slugging in pipeline–riser systems, are presented. In the simulations air and water were used as flowing fluids. The mathematical model considers continuity equations for liquid and gas phases, with a simplified momentum equation for the mixture, neglecting inertia. A drift-flux model, evaluated for the local conditions in the riser, is used as a closure law. The developed model predicts the location of the liquid accumulation front in the pipeline and the liquid level in the riser, so it is possible to determine which type of severe slugging occurs in the system. The numerical procedure is convergent for different nodalizations. A comparison is made with experimental results corresponding to a catenary riser, showing very good results for slugging cycle and stability and flow regime maps.

1. Introduction

Severe slugging is a terrain dominated phenomenon, characterized by the formation and cyclical production of long liquid slugs and fast gas blowdown. Severe slugging may appear for low gas and liquid flow rates when a section with downward inclination angle (pipeline) is followed by another section with an upward inclination (riser). This configuration is common in off-shore petroleum production systems. Main issues related to severe slugging are (Wordsworth et al., 1998): (a) high average back pressure at well head, causing tremendous production losses, (b) high instantaneous flow rates, causing instabilities in the liquid control system of the separators and eventually shutdown, and (c) reservoir flow oscillations.

For steady state and low flow rates, the flow pattern in the pipeline may be stratified, while it may be intermittent in the riser, as shown in Fig. 1a.

A cycle of severe slugging can be described as taking place according to the following stages (Taitel, 1986). Once the system destabilizes and gas passage is blocked at the bottom of the riser, liquid continues to flow in and gas already in the riser continues to flow out, being possible that the liquid level in the riser falls below the top level at the separator. As a consequence, the riser column becomes heavier and pressure at the bottom of the riser increases, compressing the gas in the pipeline and creating a liquid accumulation region. This stage is known as slug formation (Fig. 1b).

As the liquid level reaches the top while the gas passage is kept blocked at the bottom, pressure reaches a maximum and there is only liquid flowing in the riser. This is the slug production stage (Fig. 1c).

Since gas keeps flowing in the pipeline, the liquid accumulation front is pushed back until it reaches the bottom of the riser, starting the blowout stage (Fig. 1d).

As the gas phase penetrates into the riser the column becomes lighter, decreasing the pressure and then rising the gas flow. When gas reaches the top of the riser, gas passage is free through the stratified flow pattern in the pipeline and the intermitent/annular flow pattern in the riser, causing a violent expulsion and a rapid decompression that brings the process to slug formation again. This stage is known as gas blowdown (Fig. 1e).

Fig. 1f shows the different stages in the pressure history at the bottom of the riser corresponding to an experiment under laboratory conditions (Schmidt, 1977).

A classification of severe slugging can be made, according to the observed flow regime, as follows (Wordsworth et al., 1998):

- *Severe Slugging 1 (SS1):* the liquid slug length is greater to or equal to one riser length and maximum pipeline pressure is equal to the hydrostatic head of the riser (neglecting friction pressure drop).
- *Severe Slugging 2 (SS2):* the liquid length is less than one riser length, with intermittent gas penetration at the bottom of the riser.

* Corresponding author. Tel.: +55 11 3848 0127; fax: +55 11 3091 5642.
E-mail address: jlbalino@usp.br (J.L. Baliño).

0301-9322/$ - see front matter © 2010 Elsevier Ltd. All rights reserved.
doi:10.1016/j.ijmultiphaseflow.2010.04.003

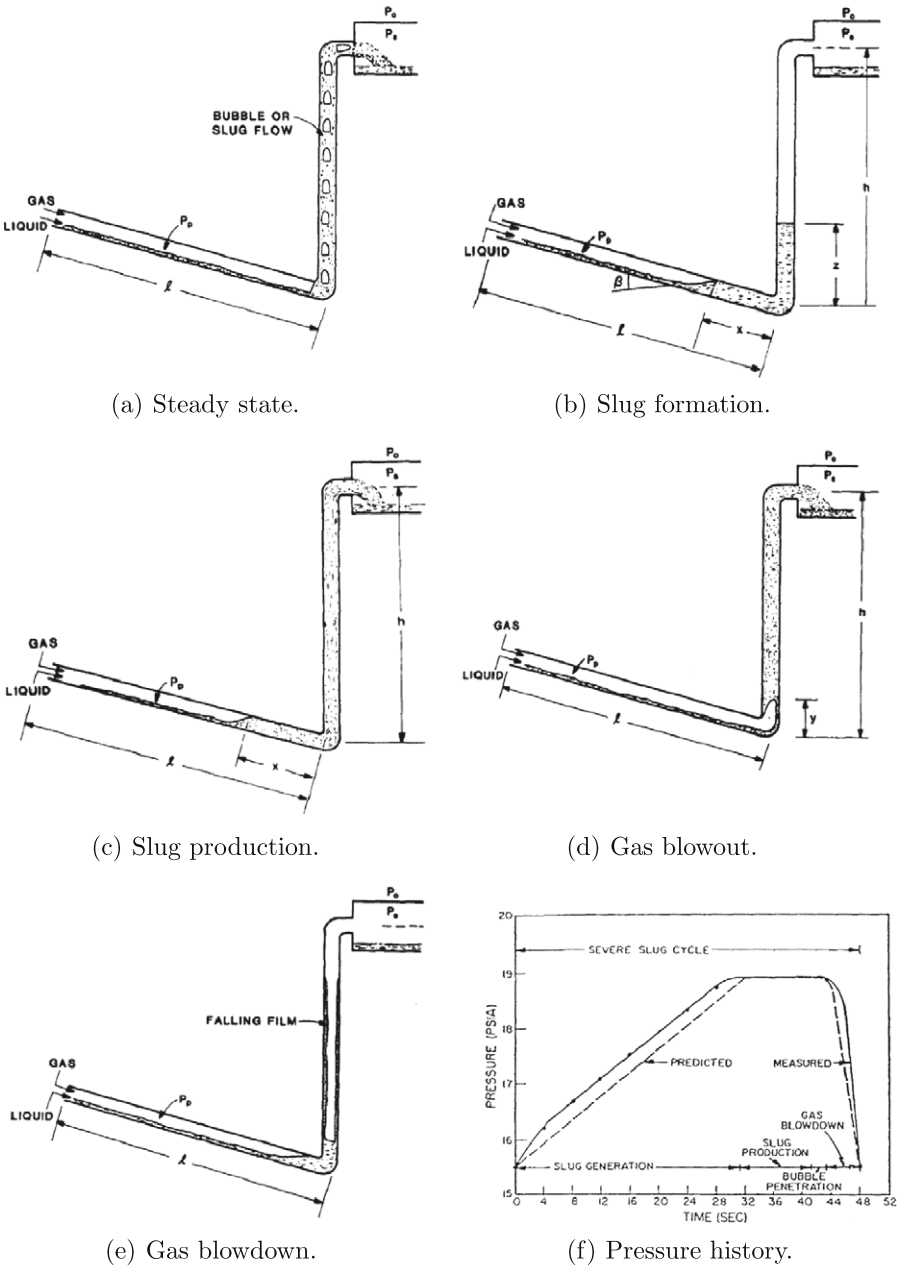

(a) Steady state. (b) Slug formation.

(c) Slug production. (d) Gas blowout.

(e) Gas blowdown. (f) Pressure history.

Fig. 1. Stages for severe slugging (from Taitel, 1986; Schmidt, 1977).

- *Severe Slugging 3 (SS3):* there is continuous gas penetration at the bottom of the riser; visually, the flow in the riser resembles normal slug flow, but pressure, slug lengths and frequencies reveal cyclic variations of smaller periods and amplitudes compared to SS1.
- *Oscillation (OSC):* there are cyclic pressure fluctuations without the spontaneous vigorous blowdown.

Most of the models for severe slugging were developed for vertical risers and assume one-dimensional, isothermal flow and a mixture momentum equation in which only the gravitational term is important.

In (Taitel et al., 1990) a model was presented considering constant mean values for the gas density and void fraction in the riser, allowing to calculate time variations of pipeline pressure, position of the accumulation region, flow rate into the riser and mean holdup. It was found that as the operation point moves closer to the stability line the numerical procedure did not converge, giving gas mass flows going to infinite as the spatial discretization was decreased. Experimental data were obtained from a facility for different buffer volumes (simulating equivalent pipeline lengths) and a comparison was made with the simulation results, showing good agreement except for the blowout/blowdown stage. Setting apart the non-convergence problems, lumped parameter models seem to work fine for short risers, where the local variations of variables are small, but are not successful in long risers, typical of offshore systems.

In (Sarica and Shoham, 1991) a model with a distributed parameter formulation for the riser was presented. Considering continuity equations for the liquid and gas without phase change and a gravity-dominant mixture momentum equation, the model was capable of handling discontinuities such as liquid accumulation in the piping and liquid level in the riser. The resulting equations were solved by using the method of characteristics. A comparison

of simulations with different experimental data showed reasonable agreement, although the model also suffered from non-convergence in the unstable region.

Wordsworth et al. (1998) presented the results of a programme of work carried out by the company CALtec on behalf of the company Petrobras. The work investigated experimentally the influence of pressure on the multiphase flow behavior in a catenary pipeline–riser system and, in particular, the initiation and characteristics of severe slugging. Air and water were used as the test fluids. Tests were carried out at pressures ranging from 1 to 15 bar g. The work led to the development of flow regime maps at pressures of 1, 2, 3 and 4 bar g which shows the location of the severe slugging and stable flow regions. No severe slugging was observed above 4 bar g. The experimental data has been used by Petrobras to test existing computer tools and to give support to the development of new modeling techniques.

The objective of this paper is to develop a model for severe slugging valid for risers with variable inclination and to use this model to simulate numerically the air–water multiphase flow in a catenary riser for the experimental conditions reported in (Wordsworth et al., 1998). Complete results of this study were presented in (Baliño, 2008). Another objective is to built stability and flow regime maps in the system parameter space for the multiphase flow in a pipeline–riser system. To accomplish this objective, a code was built based on the numerical discretization of the model equations and a series of numerical simulations were performed, according to the procedure described below.

The stationary solution for a given point in the system parameter space is given as initial condition for the numerical simulation; if the numerical solution does not go away from the initial condition with time, the stationary solution is stable and it is the system steady state. If the numerical solution goes away with time, the stationary state is unstable, there is no steady state and an intermittent solution develops with time. By changing the point in the system parameter space and repeating this process, the stability map can be built. For unstable flow, the analysis of the limit cycle leads to the determination of the flow regime map, showing the regions corresponding to the different types of intermittency.

Concerning stability analysis for severe slugging, models that lead to a stability criteria (Bœ, 1981; Taitel, 1986) have important simplifications and are not completely satisfactory even for vertical risers. On the other hand, commercial computer codes can take into account all effects but they do not incorporate stability analysis. An important motivation for this study is the future application of the linear stability theory to the developed model, in order to obtain stability maps more efficiently from the point of view of computing cost compared to procedure described in the paragraph above.

The paper is organized as follows: in Section 2 the developed model for the pipeline–riser system is presented; in Section 3 the stationary state (initial condition for the dynamic program) is shown; in Section 4 the discretization and numerical implementation of the model is shown; in Section 5 some numerical studies in order to validate the computer program are described; in Section 6 the experimental study made by Wordsworth et al. (1998) and the analysis of the experimental data are described; in Section 7 the numerical simulation are described and a comparison is made with the experimental data; in Section 8, stability and flow regime maps obtained numerically are compared with experimental results; in the last section the conclusions of the reported work are presented.

2. Model

The model considers one-dimensional flow in both pipeline and riser subsystems. The liquid phase is assumed incompressible, while the gas phase is considered as an ideal gas. Both phases flow in isothermal conditions. The flow pattern in the pipeline is assumed stratified, while in the riser inertia is neglected, resulting the NPW (no pressure wave) model (Masella et al., 1998). In this way, severe slugging is controlled mainly by gravity in the riser and compressibility in the pipeline. The model is capable of handling discontinuities in the flow, such as liquid accumulation in the pipeline, liquid level in the riser and void fraction waves.

2.1. Pipeline

The pipeline, shown in Fig. 2, can be either in a condition of liquid accumulation ($x > 0$) or in a condition of continuous gas penetration ($x = 0$), where x is the position of the liquid accumulation front. The existence of a buffer vessel with volume υ_e is considered in order to simulate an equivalent pipeline length $L_e = \frac{\upsilon_e}{A}$, where A is the flow passage area ($A = \frac{1}{4}\pi D^2$, where D is the inner diameter). Variations in the pipeline void fraction α_p are neglected during the transient. The state equations are obtained by applying continuity equations for the liquid and gas phases. For $x > 0$ they are:

$$j_{gb} = 0 \tag{1}$$

$$\frac{dx}{dt} = \frac{\frac{Q_{l0}}{A} - j_{lb}}{\alpha_p} \tag{2}$$

$$\frac{dP_g}{dt} = \frac{-P_g\left(j_{lb} - \frac{Q_{l0}}{A}\right) + \frac{R_g T_g}{A}\dot{m}_{g0}}{(L-x)\alpha_p + L_e} \tag{3}$$

$$P_b = P_g + \rho_l g x \sin\beta \tag{4}$$

where g is the gravity acceleration constant, j_{lb} and j_{gb} are, respectively, the superficial velocities for the liquid and gas at the bottom of the riser, L is the pipeline length, $\dot{m}_{g0}$ is the gas mass flow rate injected in the pipeline, P_b and P_g are, respectively, the pressure at the bottom of the riser and the gas pressure, Q_{l0} is the liquid volumetric flow injected in the pipeline, R_g and T_g are, respectively, the gas constant and temperature, t is time, ρ_l is the liquid density and β is the pipeline inclination angle (positive when downwards).

For $x = 0$ the state equations are:

$$j_{lb} = \frac{Q_{l0}}{A} \tag{5}$$

$$\frac{dP_g}{dt} = \frac{-P_g j_{gb} + \frac{R_g T_g}{A}\dot{m}_{g0}}{L\alpha_p + L_e} \tag{6}$$

The void fraction at the pipeline is determined from the following algebraic relationship evaluated for the stationary state (see Section 3), and derived from the momentum balance in stratified flow (Taitel and Dukler, 1976) (see Fig. 3):

$$\tau_{wg}\frac{S_g}{\alpha_p} - \tau_{wl}\frac{S_l}{1-\alpha_p} + \tau_i S_i\left(\frac{1}{1-\alpha_p} + \frac{1}{\alpha_p}\right) + (\rho_l - \rho_g)Ag\sin\beta = 0 \tag{7}$$

where S_g, S_i and S_l are respectively the gas, interfacial and liquid wetted perimeters, τ_{wg}, τ_i and τ_{wl} are respectively the wall-gas, interface and wall-liquid shear stresses and ρ_g is the gas density.

In Eq. (7) the wetted and interfacial perimeters are determined considering a stratified geometry, while the shear stresses are related to the superficial velocities of the phases through suitable friction factors. The representative superficial velocities for the gas and liquid (respectively $\bar{j}_g$ and $\bar{j}_l$) are calculated from the stationary state. The calculation procedure can be seen in Kokal and Stanislav (1989).

The superficial velocities must be determined when the pipeline commutes between the states of liquid accumulation and continuous gas penetration.

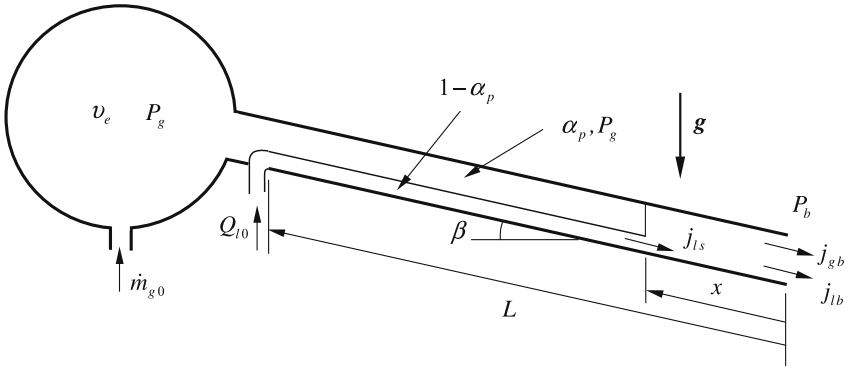

Fig. 2. Definition of variables at the pipeline.

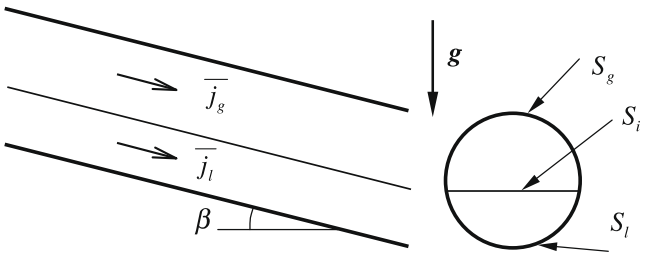

Fig. 3. Stratified flow at the pipeline.

Assuming that the commutation from the state $x > 0$ to the state $x = 0$ happens at time t_0, it can be shown that the superficial velocities at times immediately before t_0^- and immediately after t_0^+ can be determined as follows:

$$\frac{dx^+}{dt} = 0 \tag{8}$$

$$j_{gb}^- = 0 \tag{9}$$

$$j_{gb}^+ = -\alpha_p \frac{dx^-}{dt} \tag{10}$$

$$j_{lb}^+ = j_{lb}^- + \alpha_p \frac{dx^-}{dt} \tag{11}$$

Assuming that commutation from the state $x = 0$ to $x > 0$ happens at time t_0, it can be shown that the superficial velocities at times immediately before t_0^- and immediately after t_0^+ can be determined as follows:

$$j_{gb}^- = j_{gb}^+ = 0 \tag{12}$$

$$j_{lb}^+ = j_{lb}^- \tag{13}$$

$$\frac{dx^+}{dt} = 0 \tag{14}$$

In Eqs. (8)–(14) the superscripts − and + denote variables evaluated respectively at t_0^- and t_0^+. In this way, in any commutation the total superficial velocity, pressure and time derivative of the pressure at the bottom of the riser are continuous.

2.2. Riser

Continuity equations for the phases and the mixture momentum equation with an ideal and isothermal gas are considered at the riser (see Fig. 4). This results in the following set of equations:

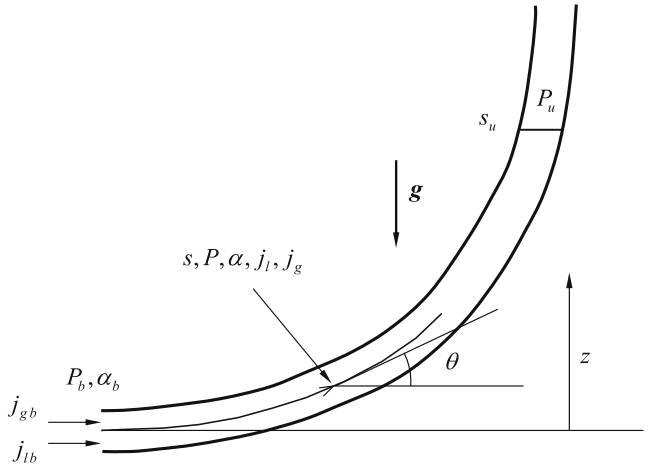

Fig. 4. Definition of variables at the riser.

$$-\frac{\partial \alpha}{\partial t} + \frac{\partial j_l}{\partial s} = 0 \tag{15}$$

$$\frac{\partial}{\partial t}(P\alpha) + \frac{\partial}{\partial s}(Pj_g) = 0 \tag{16}$$

$$\frac{\partial P}{\partial s} = -\rho_m g \sin\theta - \frac{4\tau_w}{D} \tag{17}$$

$$\rho_m = \rho_l(1-\alpha) + \rho_g \alpha \tag{18}$$

$$\rho_g = \frac{P}{R_g T_g} \tag{19}$$

where j_g and j_l are respectively the gas and liquid superficial velocities, P is the pressure, s is the position along the riser, α is the void fraction, ρ_m is the mixture density, τ_w is the wall shear stress and $\theta = \theta(s)$ is the inclination angle.

The shear stress at the wall is calculated using a homogeneous two-phase model:

$$\tau_w = \frac{1}{2} f_m \rho_m j|j| \tag{20}$$

$$f_m = f\left(Re_m, \frac{\epsilon}{D}\right) \tag{21}$$

$$Re_m = \frac{\rho_m D|j|}{\mu_m} \tag{22}$$

$$\mu_m = \mu_l(1-\alpha) + \mu_g \alpha \tag{23}$$

where f is the Fanning friction factor for the mixture, calculated from (Chen, 1979), j is the total superficial velocity, Re_m is the Rey-

nolds number of the mixture and μ_g, μ_m and μ_l are respectively the dynamic viscosities of the gas, mixture and liquid.

The pressure gradient results, finally:

$$\frac{\partial P}{\partial s} = -\rho_m \left(g \sin\theta + 2\frac{f_m}{D} j|j| \right) \tag{24}$$

The superficial velocities for the phases are determined by using a drift flux correlation, assumed to be locally valid:

$$j_g = u_g \alpha = \alpha(C_d j + U_d) \tag{25}$$

$$j_l = j - j_g = u_l(1-\alpha) = (1-\alpha C_d) j - \alpha U_d \tag{26}$$

where u_g and u_l are respectively the gas and liquid velocities. It will be assumed that the drift parameters C_d and U_d depend at most on the local flow conditions and on the inclination angle, this is, $C_d = C_d(\alpha, P, j, \theta)$ and $U_d = U_d(\alpha, P, j, \theta)$ (Bendiksen, 1984; Chexal et al., 1992).

Considering as the state variables in the riser the void fraction, pressure and total superficial velocity (functions of position and time), Eqs. (15) and (16) can be rewritten as:

$$\frac{\partial \alpha}{\partial t} + \frac{\partial j_g}{\partial \alpha}\frac{\partial \alpha}{\partial s} + \frac{\partial j_g}{\partial P}\frac{\partial P}{\partial s} + \left(\frac{\partial j_g}{\partial j} - 1\right)\frac{\partial j}{\partial s} + \frac{\partial j_g}{\partial \theta}\frac{d\theta}{ds} = 0 \tag{27}$$

$$P\frac{\partial \alpha}{\partial t} + \alpha\frac{\partial P}{\partial t} + P\frac{\partial j_g}{\partial \alpha}\frac{\partial \alpha}{\partial s} + \left(j_g + P\frac{\partial j_g}{\partial P}\right)\frac{\partial P}{\partial s} + P\frac{\partial j_g}{\partial j}\frac{\partial j}{\partial s} + P\frac{\partial j_g}{\partial \theta}\frac{d\theta}{ds} = 0 \tag{28}$$

An analysis of characteristic directions (Drew and Passman, 1999) of the system of Eqs. (17), (27) and (28) shows that there exist only one finite eigenvalue $\lambda = \frac{\partial j_g}{\partial \alpha}$, being the other two eigenvalues equal to infinite. On this ground, the model is qualified as *mixed hyperbolic/parabolic*. The number of characteristic equations associated with the infinite eigenvalues results from the facts that the superficial velocities are related through an algebraic drift relation and the pressure along the pipe can be calculated directly by integrating in position the mixture momentum equation.

The compatibility conditions (resulting equations in the propagation direction) can be written as:

$$\frac{D_g \alpha}{Dt} + \frac{\partial j_g}{\partial P}\frac{\partial P}{\partial s} + \left(\frac{\partial j_g}{\partial j} - 1\right)\frac{\partial j}{\partial s} + \frac{\partial j_g}{\partial \theta}\frac{d\theta}{ds} = 0 \tag{29}$$

$$\alpha\frac{D_g P}{Dt} + \left(j_g - \alpha\frac{\partial j_g}{\partial \alpha}\right)\frac{\partial P}{\partial s} + P\frac{\partial j}{\partial s} = 0 \tag{30}$$

where

$$\frac{D_g}{Dt} = \frac{\partial}{\partial t} + \frac{\partial j_g}{\partial \alpha}\frac{\partial}{\partial s} \tag{31}$$

The drift coefficients used in the model are (Bendiksen, 1984):

- For $Fr_j < 3.5$:

$$C_d = 1.05 + 0.15\sin\theta \tag{32}$$

$$U_d = \sqrt{gD}(0.35\sin\theta + 0.54\cos\theta) \tag{33}$$

- For $Fr_j \geqslant 3.5$:

$$C_d = 1.2 \tag{34}$$

$$U_d = 0.35\sqrt{gD}\sin\theta \tag{35}$$

where the Froude number Fr_j is defined as:

$$Fr_j = \frac{|j|}{\sqrt{gD}} \tag{36}$$

If the drift coefficients depend only on the inclination angle, as in (Bendiksen, 1984), the characteristic direction corresponds to the gas velocity $\frac{\partial j_g}{\partial \alpha} = \frac{j_g}{\alpha} = u_g$ and the compatibility conditions simplify to:

$$\frac{D_g \alpha}{Dt} + \alpha\frac{\partial}{\partial s}(C_d j + U_d) - \frac{\partial j}{\partial s} = 0 \tag{37}$$

$$\alpha\frac{D_g P}{Dt} + P\frac{\partial j}{\partial s} = 0 \tag{38}$$

Eqs. (37) and (38) can be regarded as a generalization of the characteristic equations presented in (Sarica and Shoham, 1991) to risers of variable inclination. The values for C_d and U_d chosen for simulations in vertical risers in (Sarica and Shoham, 1991) are constant.

2.3. Coupling between pipeline and riser

Assuming the same flow passage area for the pipeline and riser, the pressure and superficial velocities at the bottom of the riser are continuous:

$$P(s=0,t) = P_b(t) \tag{39}$$

$$j_g(s=0,t) = j_{gb}(t) \tag{40}$$

$$j_l(s=0,t) = j_{lb}(t) \tag{41}$$

The boundary condition for the void fraction can be obtained from Eq. (25) evaluated at the bottom of the riser:

$$\alpha(s=0,t) = \alpha_b(t) = \frac{j_{gb}}{C_{db} j_b + U_{db}} \tag{42}$$

Fig. 5 shows the state variables and the coupling between the subsystems. State variables for the pipeline are the gas pressure and position of the liquid accumulation front, while for the riser they are the local pressure, void fraction and total superficial velocity. The pipeline imposes pressure and void fraction at the bottom of the riser, while the riser imposes the total superficial velocity to the pipeline; these variables are the boundary conditions for the corresponding subsystems. Additional boundary conditions are the liquid volumetric flow rate and the gas mass flow rate at the pipeline, as well as the separation pressure at the top of the riser.

2.4. Catenary geometry

The catenary geometry is characterized by the coordinates X and Z corresponding to the top of the riser, assuming that the incli-

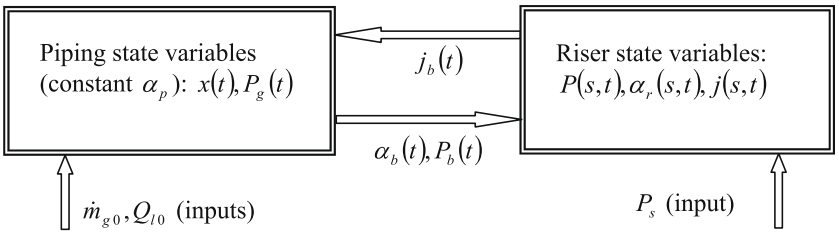

Fig. 5. Coupling between subsystems.

nation angle at the bottom is zero. The local height z of a point belonging to the catenary can be written as:

$$z = a\left[\cosh\left(\frac{x}{a}\right) - 1\right] \tag{43}$$

where the dimensional catenary constant a is obtained as the solution of the following transcendental equation:

$$Z = a\left[\cosh\left(\frac{X}{a}\right) - 1\right] \tag{44}$$

The local position s along the catenary and the top position s_t result:

$$s = a\sinh\left(\frac{x}{a}\right) \tag{45}$$

$$s_t = a\sinh\left(\frac{X}{a}\right) \tag{46}$$

The local inclination angle θ results:

$$\theta = \arg\tan\left[\sinh\left(\frac{x}{a}\right)\right] \tag{47}$$

Knowing the position s, the abscissa x can be calculated from (45):

$$x = a\arg\sinh\left(\frac{s}{a}\right) \tag{48}$$

3. Stationary state

The stationary state is important since it is used as the initial condition for the transient simulations and also as the base solution for the linear stability analysis. The stationary state can be obtained by setting to zero the time derivatives in the dynamic equations. Variables at stationary state are denoted with superscript $\tilde{}$. The stationary state exists only for the state $x = 0$.

For the pipeline, as $x = 0$, Eqs. (5) and (6) give:

$$\tilde{j}_{lb} = \frac{Q_{l0}}{A} \tag{49}$$

$$\tilde{P}_g\tilde{j}_{gb} = \frac{R_g T_g \dot{m}_{g0}}{A} \tag{50}$$

For the riser, Eqs. (15) and (16) and coupling conditions (39)–(41) give:

$$\tilde{j}_l = \tilde{j}_{lb} = \frac{Q_{l0}}{A} \tag{51}$$

$$\widetilde{P}\tilde{j}_g = \tilde{P}_g\tilde{j}_{gb} = \frac{R_g T_g \dot{m}_{g0}}{A} \tag{52}$$

The void fraction in the riser can be calculated from Eq. (25) as:

$$\tilde{\alpha} = \frac{R_g T_g \dot{m}_{g0}}{\widetilde{C}_d R_g T_g \dot{m}_{g0} + (Q_{l0}\widetilde{C}_d + \widetilde{U}_d A)\widetilde{P}} \tag{53}$$

The pressure distribution can be calculated by numerically integrating Eq. (17), as all terms are functions of pressure and the inclination angle is a function of position.

It can be shown (Burr and Baliño, 2007) that a closed implicit solution can be obtained for the pressure distribution in a vertical riser $\left(\theta = \frac{\pi}{2}\right)$ of height Z, neglecting friction and assuming constant drift flux parameters; these are the assumptions made in (Sarica and Shoham, 1991). The final expression is:

$$C_1(\widetilde{P} - P_s) + C_2 \ln\left(\frac{C_3 + C_4\widetilde{P}}{C_3 + C_4 P_s}\right) = Z - z \tag{54}$$

where

$$C_1 = \frac{Q_{l0}\widetilde{C}_d + \widetilde{U}_d A}{g[\dot{m}_{g0} + \rho_l(Q_{l0}\widetilde{C}_d + \widetilde{U}_d A)]} \tag{55}$$

$$C_2 = \frac{\dot{m}_{g0} R_g T_g[\rho_l(Q_{l0}\widetilde{C}_d + \widetilde{U}_d A) + \widetilde{C}_d \dot{m}_{g0}]}{g[\dot{m}_{g0} + \rho_l(Q_{l0}\widetilde{C}_d + \widetilde{U}_d A)]^2} \tag{56}$$

$$C_3 = \rho_l \dot{m}_{g0} R_g T_g(\widetilde{C}_d - 1) \tag{57}$$

$$C_4 = \dot{m}_{g0} + \rho_l(Q_{l0}\widetilde{C}_d + \widetilde{U}_d A) \tag{58}$$

4. Discretization

For the condition $x > 0$, the discretized equations for the pipeline are, from Eq. (2)–(4):

$$j_{lb}^{K+1} = j_b^{K+1} \tag{59}$$

$$j_{gb}^{K+1} = 0 \tag{60}$$

$$x^{K+1} = x^K + \frac{\frac{Q_{l0}}{A} - j_{lb}^{K+1}}{\alpha_p}\Delta t^K \tag{61}$$

$$P_g^{K+1} = \frac{P_g^K + \frac{\dot{m}_{g0} R_g T_g \Delta t^K}{A[(L - x^{K+1})\alpha_p + L_e]}}{1 + \frac{\left(j_{lb}^{K+1} - \frac{Q_{l0}}{A}\right)\Delta t^K}{(L - x^{K+1})\alpha_p + L_e}} \tag{62}$$

$$P_b^{K+1} = P_g^{K+1} + \rho_l g x^{K+1}\sin\beta \tag{63}$$

where Δt^K is the time step and the superscripts K and $K+1$ denote variables correspondingly at times t^K and $t^{K+1} = t^K + \Delta t^K$.

For the condition $x = 0$, the discretized equations for the pipeline are, from Eqs. (5) and (6):

$$j_{lb}^{K+1} = \frac{Q_{l0}}{A} \tag{64}$$

$$j_{gb}^{K+1} = j_b^{K+1} - \frac{Q_{l0}}{A} \tag{65}$$

$$P_g^{K+1} = \frac{P_g^K + \frac{\dot{m}_{g0} R_g T_g \Delta t^K}{A(L\alpha_p + L_e)}}{1 + \frac{j_{gb}^{K+1}\Delta t^K}{L\alpha_p + L_e}} \tag{66}$$

$$P_b^{K+1} = P_g^{K+1} \tag{67}$$

In the riser a moving grid method was adopted, in which node i $(1 \leqslant i \leqslant N-1)$ moves with the corresponding characteristic (gas) velocity. Last node N moves with the liquid velocity if the liquid level falls below the top of the riser ($s_u < s_t$), or remains fixed at position s_t otherwise. The time step Δt^k is chosen as the time step such that the characteristic propagated from the $N-1$th node intersects the position s_u at time $t^k + \Delta t^k$ if the liquid level falls below the top level in the riser, or as the time step such that the characteristic propagated from the $N-1$th node intersects position s_t otherwise. The velocity of the liquid level $u_{l\,u}$ can be calculated from Eq. (26) evaluated at the liquid level position s_u:

$$u_{lu} = \frac{ds_u}{dt} = \frac{(1 - \alpha_u C_{du})j_u - \alpha_u U_{du}}{1 - \alpha_u} \tag{68}$$

As the gas velocity is positive, a node disappears at the liquid level or top of the riser and a node is created at the bottom of the riser, keeping constant the number of nodes.

An algorithm was devised to adjust the total superficial velocity at the last riser node in order to satisfy the separator pressure boundary condition in the converged solution.

Eqs. (37) and (38) were discretized and integrated along the characteristic direction with the gas velocity (nodes 1 and 2 in Fig. 6) using a backward difference for the space derivatives, while Eq. (24) was integrated between nodes $2L$ (located at the left of

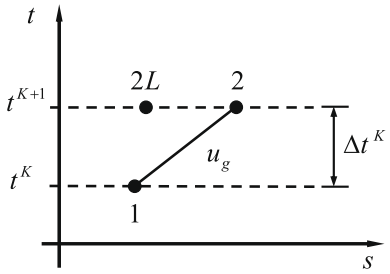

Fig. 6. Discretization along the characteristic directions.

node 2) and 2. An implicit scheme was used, with a predictor–corrector method for treatment of the nonlinearities.

Position of node 2 is calculated as:

$$s_2 = s_1 + u_{g2}\Delta t^K \tag{69}$$

From Eq. (38) it results:

$$j_{2L} = j_2 + \frac{\alpha_2}{P_2}\frac{P_2 - P_1}{\Delta t^K}\Delta s_{2L} \tag{70}$$

where

$$\Delta s_{2L} = s_2 - s_{2L} \tag{71}$$

From Eq. (37) it results:

$$\alpha_2 = \frac{\alpha_1 + \left(\frac{\partial j}{\partial s}\right)_2 \Delta t^K}{1 + \left[\frac{\partial}{\partial s}(C_d j + U_d)\right]_2 \Delta t^K} \tag{72}$$

where

$$\left(\frac{\partial j}{\partial s}\right)_2 = \frac{j_2 - j_{2L}}{\Delta s_{2L}} \tag{73}$$

$$\left[\frac{\partial}{\partial s}(C_d j + U_d)\right]_2 = \frac{(C_d j + U_d)_2 - (C_d j + U_d)_{2L}}{\Delta s_{2L}} \tag{74}$$

From Eq. (24) it results:

$$P_2 = \frac{P_{2L} - \rho_l(1-\alpha_2)\Delta E_2}{1 + \frac{\alpha_2}{R_g T_g}\Delta E_2} \tag{75}$$

where

$$\Delta E_2 = g\Delta z_2 + \frac{2f_{m2}}{D} j_2 |j_2| \Delta s_2 \tag{76}$$

$$\Delta z_2 = z_2 - z_{2L} \tag{77}$$

The calculation procedure can be summarized as follows:

(1) Define guess values for variables at t^{K+1} based on known values at time t^K.
(2) Determine Δt^K and calculate positions of nodes at t^{K+1} from Eq. (69).
(3) Calculate total superficial velocity at time t^{K+1} for nodes $N-1$ to 1 from Eq. (70). The total superficial velocity at node 1 is an input to the pipeline subsystem.
(4) Calculate the void fraction at time t^{K+1} for nodes N to 2 from Eq. (72).
(5) Calculate P_g^{K+1}, P_b^{K+1} (input to the riser subsystem), x^{K+1}, j_{gb}^{K+1} and j_{lb}^{K+1} from the suitable pipeline relations, Eqs. (59)–(67). Calculate the void fraction at the bottom of the riser α_b^{K+1} (input to the riser subsystem) from Eq. (42).
(6) Check convergence of state variables and pressure boundary condition at the separator by a comparison with pressure at riser node N. If convergence is not achieved, modify the total superficial velocity at node N, update state variables and go to item 2 until convergence is achieved.

A computer program was developed for calculating the stationary state and the transient.

5. Program validation

A convergence study was made, varying the number of nodes. The following parameters were chosen for a comparison with an example given by Sarica and Shoham (1991), simulating experimental data of Jansen (1990) for a vertical riser: fluid parameters are $\mu_l = 1. \times 10^{-3}$ kg/m/s, $\mu_g = 1.8 \times 10^{-5}$ kg/m/s, $\rho_l = 1. \times 10^3$ kg/m^3, $R_g = 287$ m^2/s^2/K and $T_g = 20$ °C; pipeline parameters are $L = 9.14$ m, $L_e = 9.5$ m and $\beta = 1°$; riser height is $Z = 3$ m; common parameters for pipeline and riser are $D = 2.54 \times 10^{-2}$ m and $\epsilon = 1.5 \times 10^{-6}$ m; flow parameters are $j_{g0} = 0.069$ m/s, $j_{l0} = 0.146$ m/s and $P_s = 1.013$ bar a. The superficial velocities j_{g0} and j_{l0} at standard conditions (pressure $P_0 = 1.013$ bar a, temperature $T_0 = 20$ °C) are related to the flows as:

$$j_{g0} = \frac{R_g T_0 \dot{m}_{g0}}{P_0 A} \tag{78}$$

$$j_{l0} = \frac{Q_{l0}}{A} \tag{79}$$

Table 1 shows simulation results corresponding to nodalizations ranging from 6 to 201 nodes. It can be observed an excellent convergence on period T, pressure amplitude at the bottom of the riser ΔP, maximum penetration of the liquid front in the pipeline x_{max}, minimum liquid height at the riser $z_{u\,min}$ and maximum void fraction at the liquid level in the riser $\alpha_{u\,max}$; convergence is attained more slowly for the maximum gas superficial velocity $j_{gu\,max}$ at the liquid level in the riser. Acceptably converged results can be observed with $N = 51$ nodes.

It is important to notice that, as the method of characteristics satisfies the Courant–Friedrichs–Levy (CFL) stability condition (Tannehill et al., 1997) and as the characteristic direction u_g is not constant, in the calculation procedure described in Section 4 the time step is dependent on the nodalization and it is not constant along the simulation. Times steps are considerably shorter in the blowout/blowdown stages than in the slug formation/production stages. Table 1 also shows the minimum and maximum times steps resulting in the simulation.

The following figures show the transient simulations corresponding to different variables necessary to characterize the type of severe slugging: pressure at the bottom of the riser (Fig. 7), void fraction at the bottom of the riser (Fig. 8), void fraction at the liquid level in the riser (Fig. 8a), gas superficial velocity (Fig. 8b) and liquid superficial velocity (Fig. 8c) at the bottom of the riser, gas superficial velocity (Fig. 8d) and liquid superficial velocity (Fig. 8e) at the liquid level in the riser, position of liquid accumulation front (Fig. 8f) and position of liquid level at the riser (Fig. 8g). It can be seen that, in this case, the stationary state used as the initial condition is not stable and the system goes to a limit cycle.

From the simulation run with 51 nodes and considering that the slugging cycle begins when the gas passage at the bottom of the riser is blocked, times corresponding to different stages described in Section 1 were calculated, such as the slug formation time (24.1 s), slug production time (25.1 s), bubble penetration time (2.2 s) and gas blowdown time (0.9 s). The slug length were calculated by integrating the liquid superficial velocity at the top of the riser in the period in which the void fraction is zero, resulting $L_s = 7.09$ m; as $L_s > Z$, this transient characterizes a severe slugging type 1 (Wordsworth et al., 1998). In this case, the liquid level can be lower than the top of the riser (there is liquid fallback). The relatively short period of time corresponding to the blowout/blowdown stages (3.1 s), in which the gas superficial velocity changes

Table 1
Convergence study for different number of nodes.

N	Δt_{min} (s)	Δt_{max} (s)	T (s)	ΔP (bar)	x_{max} (m)	$z_{u\,min}$ (m)	$j_{gu\,max}$ (m/s)	$\alpha_{u\,max}$ (–)
6	0.201	2.56	53.9	0.211	1.90	1.47	1.61	0.735
11	0.0687	1.52	53.0	0.216	1.91	1.26	2.27	0.757
21	0.0260	0.775	53.0	0.219	1.91	1.19	2.87	0.771
51	0.00995	0.293	52.3	0.220	1.91	1.14	3.13	0.776
101	0.00495	0.148	52.1	0.220	1.91	1.12	3.23	0.777
151	0.00322	0.102	52.1	0.220	1.91	1.12	3.26	0.778
201	0.00246	0.0866	52.1	0.220	1.91	1.12	3.28	0.778

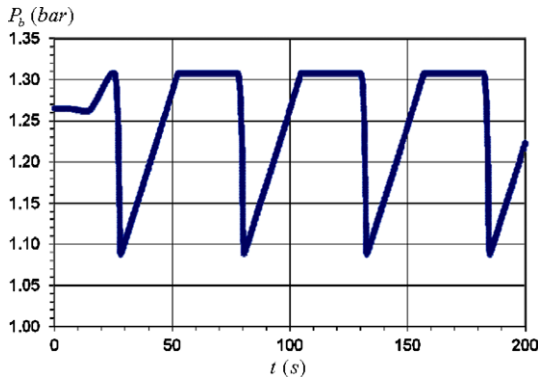

Fig. 7. Simulated pressure transient at the bottom of the riser, convergence study, $N = 51$.

dramatically, is the reason why the convergence on this variable is not as fast as on the others.

Sarica and Shoham (1991) reported a significant influence of the time step, which was kept constant in the simulation, on cycle periods, maximum liquid penetration length in the pipeline and pressure amplitude at the bottom of the riser. Results were presented for time steps of 1.0 and 0.1 s, but no information was given about the nodalization. From Table 1, it can be seen that a time step of 0.1 s would not satisfy the CFL stability condition in the blowout/blowdown simulation stages for grids with 11 nodes or finer. On the other hand, simulations in (Taitel et al., 1990) were made with 51 nodes and the time step was adjusted in order to satisfy the CFL stability condition.

The mean experimental values for slugging period and pressure amplitude, read from the graphs in Sarica and Shoham (1991), were $T_{exp} = 42.4$ s and $\Delta P_{exp} = 0.223$ bar. The simulated slugging period ($T_{sim} = 52.3$ s) slightly overpredicts the experimental one, but is slightly better (closer to the experimental value) than the cycle times obtained with the models of Taitel et al. (1990), Sarica and Shoham (1991). The simulated pressure amplitude ($\Delta P_{sim} = 0.220$ bar) agrees excellently, considering that the experimental values have some dispersion.

As was stated in Section 1, the numerical procedures developed by Taitel et al. (1990), Sarica and Shoham (1991) suffer of non-convergence problems. A possible explanation given by Sarica and Shoham is that, below the stability line, the system loses its gravity dominance and other forces become important in the momentum equation.

A riser model with a simplified momentum equation in which only the gravity force is considered has limitations to deal with boundary conditions. In particular, for such a model to handle a discontinuous pressure boundary condition, it should react with a discontinuous time variation in the void fraction distribution; to do so, distributional (Dirac's delta) superficial velocities would be necessary. A gravity dominant riser behaves like an ideal mechanical spring, which reacts with a distributional velocity (whose time integral is a displacement) to a discontinuous applied force.

In our model, for severe slugging simulations in which the separation pressure is constant, continuity in pressure (and also in pressure time derivative) at the bottom of the riser is assured by the pipeline switching conditions detailed in Section 2.1. The implicit numerical procedure used to solve the model equations (including the time step and the gas velocity used to displace the nodes in the nonlinear iterations) also contributes to the numerical stability and convergence.

The simplified friction term implemented in our model improves the accuracy of the results and has an stabilizing effect for simulations in which discontinuous pressure boundary conditions appear, for instance in situations where a choke valve exists at the top of the riser; in the slug formation stage, pressure drop across the choke valve is negligible for gas flow only, but becomes important when the mixture level reaches the top of the riser. For these cases, discontinuous superficial velocities appear, giving maybe unrealistic but convergent results.

The model was used to simulate experimental data reported in the literature for vertical risers (Vierkandt (1988), Jansen (1990)), resulting in better results than the ones reported by using the models developed by Taitel et al. (1990), Sarica and Shoham (1991). The model was also successfully used to simulate experimental data corresponding to catenary risers (Wordsworth et al. (1998), Mokhatab (2007)).

As an example, a comparison is made for experimental data of Jansen (1990) corresponding to the same parameters as the beginning of this Section, for different superficial velocities. Table 2 shows experimental results for cycle time and pressure amplitude at the bottom of the riser (read from the pressure transients presented by Sarica and Shoham) and the corresponding values and other parameters from the simulations using the present model. Table 2 also shows cycle times and maximum penetration of the liquid front at the pipeline, as presented by Sarica and Shoham using the models of Taitel et al. (1990) and Sarica and Shoham (with $\Delta t = 0.1$ s).

In the following sections the experimental data of Wordsworth et al. (1998) (unpublished in journals) will be presented and a detailed analysis using the model will be made.

6. Data of Wordsworth et al. (1998)

Fig. 9 shows a schematic of the riser test facility with the instrumentation.

The water is supplied from a 10 m^3 storage tank, which also acts as a receiver for the water returning from the test loop. Water is delivered into the test loop using two pumps which can be operated either individually or in series. The first is a positive displacement pump with a 35 m^3/h capacity and a maximum discharge pressure of 6 bar, while the second is a single-stage centrifugal pump with 200 gpm capacity and a maximum discharge pressure of 15.2 bar. The water is metered using one of two magnetic flow-

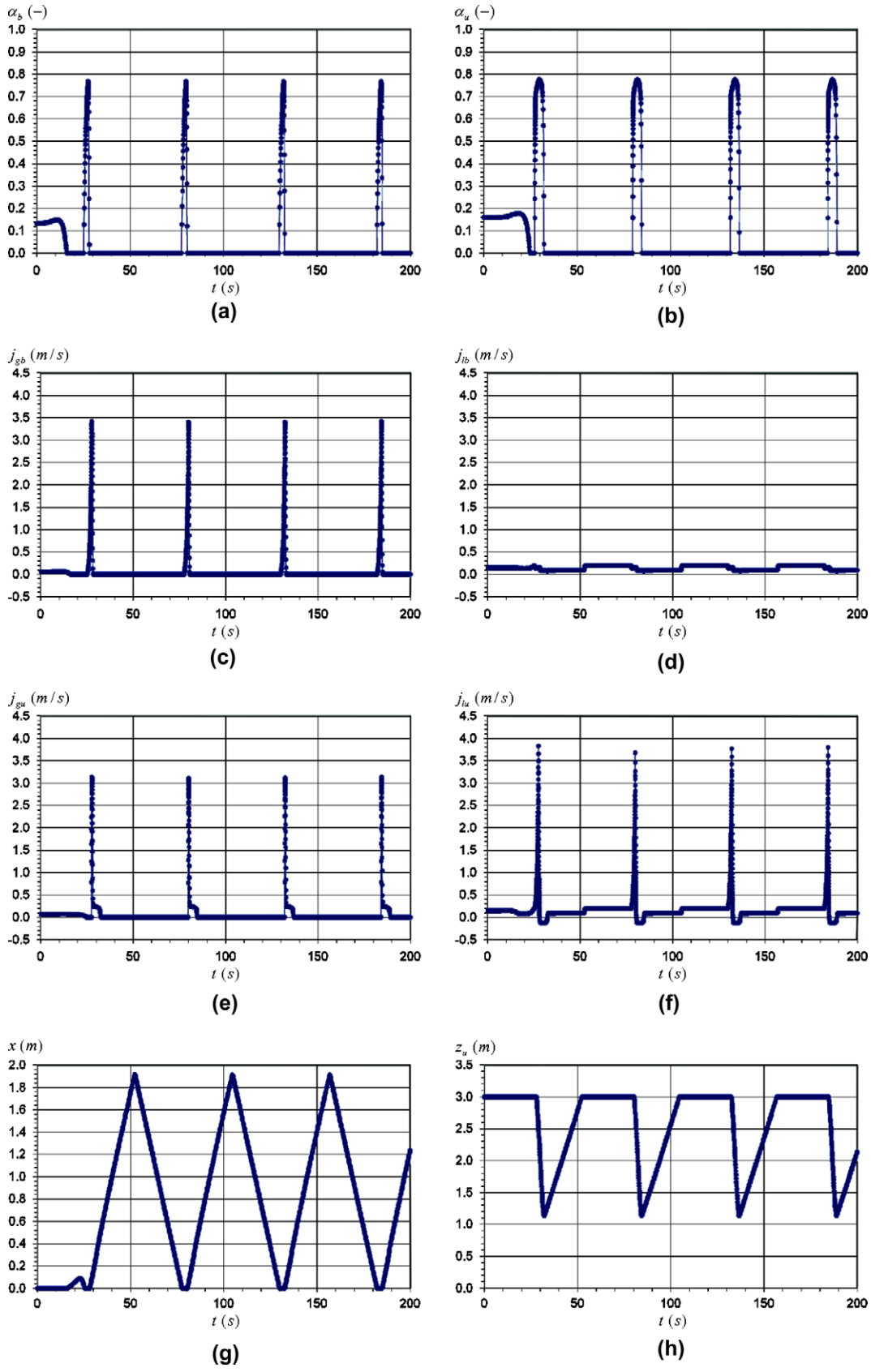

Fig. 8. Simulated transients, convergence study, $N = 51$.

meters which are located between P1 and P3. The water then passes into the test loop.

Air is supplied from a reciprocating compressor with a maximum capacity of 350 ft^3/min FAD at 18 bar. The compressor

Table 2
Comparison with experimental results (Jansen, 1990).

Experiment				Taitel et al.		Sarica and Shoham		Present model			
j_{g0} (m/s)	j_{l0} (m/s)	T_{exp} (s)	ΔP_{exp} (bar)	T (s)	x_{max} (m)	T	x_{max} (m)	T (s)	ΔP (bar)	x_{max} (m)	$z_{u\,min}$ (m)
0.069	0.146	42.4	0.220	55.9	2.12	54.7	2.03	52.3	0.223	1.91	1.14
0.116	0.066	33.8	0.211	0	0	38.0	0	36.7	0.223	0.01	0.93
0.079	0.065	40.8	0.239	52.7	0.52	52.5	0.515	51.6	0.231	0.49	0.86
0.171	0.146	26.3	0.223	22.6	0.52	22.8	0.514	22.6	0.223	0.48	1.23
0.275	0.155	14.6	0.146	0	0	15.0	0	15.2	0.190	0.03	1.64
0.256	0.053	15.0	0.058	0	0	20.2	0	19.5	0.082	0	2.13
0.354	0.054	NA	0.043	0	0	12.0	0	12.4	0.044	0	2.71

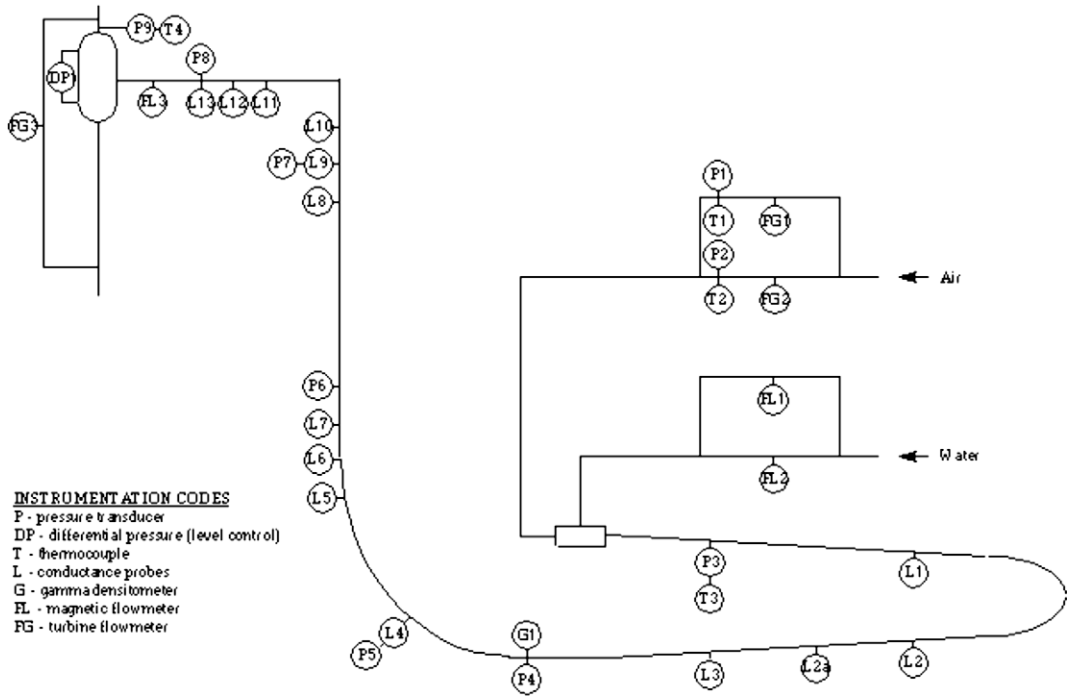

Fig. 9. Schematic of the test facility (Wordsworth et al., 1998).

supplies air into a 2.57 m^3 buffer vessel which acts as an air receiver and smooths out any pressure fluctuations from the compressor. Gas flowrates are controlled using a needle valve downstream of the air receiver. The air then passes into the metering section where the flowrate is measured using one of two turbine flowmeters, it then enters the test loop through a mixing chamber where it is mingled with the water.

The test loop consists of a 57.4 m long, 2 in. diameter pipeline which is inclined to $-2°$ from the horizontal, connected to a 9.9 m high, 2 in. catenary riser. Both the pipeline and riser are fabricated from carbon steel flanged sections and is rated to schedule 40 with flanges rated to class 300. After the test section, the two-phase mixture flows into a separator situated at the top of the riser. The separator separates the mixture into a liquid and gas line, with the gas exiting the separator at the top of vessel, where it is metered. The liquid exits the vessel through an actuated valve at the base of the separator and is sent to the storage tank. The water level in the separator is controlled with the use of a differential pressure sensor, the output of which is supplied to a process controller which controls the operation of the actuator valve.

The loop contains 9 pressure transducers, 2 in the air metering section, 2 in the horizontal section of the pipeline and 5 in the riser. A gamma densitometer is situated at the base of the riser and is used to measure the liquid hold-up. Slug progression is monitored using 14 conductance probes, situated in different positions in the system. Temperature within the riser is also monitored in 4 positions, 2 in the gas metering lines, 1 in the horizontal pipeline with the final sensor being located at the top of the separator. The signals from the instrumentation are sent to the data acquisition system. A typical measurement time was 1500 s, with a sampling rate of 10 Hz.

Tables 3–5 show experimental results obtained respectively for nominal separation pressures of 1, 2 and 3 bar g. The mean values and deviations corresponding to the separation pressure, temperature and superficial velocities were calculated from the data signals.

The pressure amplitude at the bottom of the riser for the experimental data ΔP_{exp} was measured directly from the pressure history at the bottom of the riser. As it will be explained in this Section, for the cases in which there was not a clear signal, the maximum pressure amplitude was considered (identified with the expression "max" in Tables 3–5). Regarding the experimental void fraction at the pipeline $\alpha_{p\,exp}$, the mean values are shown, except for some cases in which maximum values are given (identified with the expression "max" in Tables 3–5).

Figs. 10–16 show time evolutions for inlet air and water standard volumetric flowrates and pressures at the bottom of the riser and separator corresponding to different types of severe slugging

Table 3
Comparison with experimental results for P_s = 1 bar g (Wordsworth et al., 1998).

Case	Experiment								Simulation					
	P_s (bar a)	T (°C)	j_{g0} (m/s)	j_{l0} (m/s)	Type	ΔP_{exp} (bar)	$\alpha_{p\,exp}$ (–)	T_{exp} (s)	T_{sim} (s)	Error (%)	ΔP_{sim} (bar)	$\alpha_{p\,sim}$ (–)	x_{max} (m)	$s_{u\,min}$ (m)
1	2.03 ± 0.05	19.6 ± 0.1	1.14 ± 0.07	0.300 ± 0.009	OSC	Max 0.65	0.70	50.6	38.1	−25	0.70	0.71	0	7.46
2	2.08 ± 0.03	19.7 ± 0.1	0.11 ± 0.01	0.528 ± 0.008	SS1	0.51	Max 0.55	85.6	80.4	−6	0.22	0.56	2.92	s_t
3	2.04 ± 0.05	20.1 ± 0.1	0.07 ± 0.02	0.26 ± 0.02	SS1	0.74	Max 0.70	228	397	74	0.59	0.73	8.75	7.94
4	1.93 ± 0.05	21.4 ± 0.1	0.07 ± 0.01	0.13 ± 0.05	SS1	0.95	Max 0.84	271	556	105	0.79	0.83	11.08	4.29
5	1.69 ± 0.07	18.6 ± 0.1	0.13 ± 0.03	0.10 ± 0.07	SS1	0.99	Max 0.82	291	335	15	0.81	0.86	8.09	3.87
6	2.01 ± 0.07	19.7 ± 0.1	0.72 ± 0.08	0.29 ± 0.02	SS3	0.90	Max 0.81	62.9	52.7	−16	0.72	0.71	2.14	6.64
7	2.01 ± 0.06	21.7 ± 0.1	0.65 ± 0.05	0.18 ± 0.02	SS3	Max 0.80	0.70	80.4	67.4	−16	0.77	0.79	0.76	5.65
8	2.01 ± 0.06	22.0 ± 0.1	0.19 ± 0.03	0.16 ± 0.04	SS3	0.90	Max 0.82	151	211	40	0.79	0.83	6.53	4.44
9	1.96 ± 0.05	17.2 ± 0.5	0.41 ± 0.04	0.10 ± 0.05	SS3	Max 0.87	Max 0.80	112	119	1	0.81	0.87	0.08	4.45
10	1.95 ± 0.05	18.7 ± 0.2	0.41 ± 0.04	0.11 ± 0.05	SS3	Max 0.78	Max 0.80	113	119	1	0.81	0.87	0.06	4.45
11	2.01 ± 0.07	19.8 ± 0.1	0.48 ± 0.06	0.28 ± 0.03	SS3	0.86	Max 0.76	76	72.2	−1	0.72	0.72	4.16	6.33
12	2.01 ± 0.07	20.0 ± 0.1	0.28 ± 0.03	0.28 ± 0.03	SS3	0.83	Max 0.70	94.6	120	27	0.70	0.72	6.98	6.20
13	2.06 ± 0.05	20.0 ± 0.1	1.16 ± 0.06	0.547 ± 0.003	OSC	Max 0.69	0.75	19.3–33.8	26.8	NA	0.63	0.55	1.39	10.18
14	2.08 ± 0.07	18.7 ± 0.1	1.86 ± 0.04	0.82 ± 0.01	SF	NA	0.74	NA	Stable	NA	0	0.39	0	s_t
15	2.07 ± 0.04	20.0 ± 0.1	0.73 ± 0.04	0.546 ± 0.005	OSC	Max 0.66	0.50	25.3–41.9	35.3	NA	0.57	0.55	3.16	10.81
16	1.94 ± 0.04	18.7 ± 0.1	0.114 ± 0.004	1.39 ± 0.01	PF	NA	0.15	NA	Stable	NA	0	0.27	0	s_t
17	2.06 ± 0.03	18.7 ± 0.1	0.46 ± 0.03	0.84 ± 0.04	OSC	0.60	Max 0.52	21.8	23.7	9	0.25	0.37	0.80	s_t
18	2.05 ± 0.06	19.9 ± 0.1	0.45 ± 0.03	0.540 ± 0.007	OSC	0.57	Max 0.63	32.0	45.7	43	0.48	0.55	4.48	11.63
19	2.07 ± 0.04	19.8 ± 0.1	0.27 ± 0.02	0.536 ± 0.009	OSC	0.62	Max 0.57	47.6	59.2	24	0.39	0.55	4.43	s_t
20	2.05 ± 0.03	18.5 ± 0.1	0.25 ± 0.01	0.85 ± 0.03	OSC	0.37	Max 0.46	28.7	25.9	−10	0.15	0.37	0.67	s_t
21	2.07 ± 0.02	19.8 ± 0.1	0.09 ± 0.01	0.76 ± 0.02	OSC	Max 0.32	Max 0.49	32.9–65.8	35.5	NA	0.08	0.42	0.66	s_t

Table 4
Comparison with experimental results for P_s = 2 bar g (Wordsworth et al., 1998).

Case	Experiment								Simulation					
	P_s (bar a)	T (°C)	j_{g0} (m/s)	j_{l0} (m/s)	Type	ΔP_{exp} (bar)	$\alpha_{p\,exp}$ (–)	T_{exp} (s)	T_{sim} (s)	Error (%)	ΔP_{sim} (bar)	$\alpha_{p\,sim}$ (–)	x_{max} (m)	$s_{u\,min}$ (m)
1	2.62 ± 0.05	18.4 ± 0.1	0.46 ± 0.03	0.16 ± 0.02	SS3	0.73	0.83	81.4	92.3	13	0.73	0.82	1.84	5.72
2	2.62 ± 0.05	17.8 ± 0.1	0.21 ± 0.02	0.11 ± 0.04	SS3	0.76	0.83	119	200	68	0.74	0.86	4.08	5.04
3	2.69 ± 0.07	17.7 ± 0.1	0.50 ± 0.04	0.32 ± 0.01	SS2	Max 0.92	0.73	66.7	58.2	−13	0.55	0.69	3.07	9.33
4	2.65 ± 0.05	18.0 ± 0.1	0.10 ± 0.02	0.13 ± 0.04	SS2	0.87	0.83	170	322	89	0.59	0.83	6.24	6.93
5	2.62 ± 0.05	18.4 ± 0.1	0.26 ± 0.03	0.14 ± 0.04	SS2	0.83	0.83	116	145	25	0.71	0.83	3.96	5.69
6	2.64 ± 0.05	19.0 ± 0.1	0.12 ± 0.04	0.10 ± 0.05	SS2	0.93	0.88	225	334	48	0.71	0.87	5.82	5.27
7	2.69 ± 0.06	17.6 ± 0.1	0.30 ± 0.03	0.30 ± 0.02	SS2	0.83	0.72	76.1	80.7	6	0.47	0.70	3.93	10.19
8	2.69 ± 0.04	17.8 ± 0.1	0.07 ± 0.02	0.29 ± 0.01	SS1	0.68	0.71	109	137	26	0.19	0.71	2.32	s_t
9	2.64 ± 0.05	18.5 ± 0.1	0.06 ± 0.02	0.10 ± 0.05	SS1	0.94	0.89	301	560	86	0.65	0.87	7.06	6.13
10	2.76 ± 0.02	16.4 ± 0.1	0.104 ± 0.007	0.57 ± 0.02	SS1	Max 0.48	0.59	63.0	44.5	−29	0.09	0.54	0.67	s_t
11	2.73 ± 0.04	17.4 ± 0.2	0.10 ± 0.01	0.26 ± 0.02	SS1	0.71	0.72	126	143	13	0.28	0.73	3.32	12.07
12	2.70 ± 0.04	17.8 ± 0.1	0.03 ± 0.02	0.29 ± 0.02	SS1	0.69	0.71	136	153	13	0.09	0.71	1.18	s_t
13	2.71 ± 0.03	16.5 ± 0.1	0.70 ± 0.01	0.84 ± 0.01	SLUG	NA	0.65	NA	Stable	NA	0	0.37	0	s_t
14	2.66 ± 0.05	16.6 ± 0.1	0.14 ± 0.01	1.38 ± 0.01	SLUG	NA	0.30	NA	Stable	NA	0	0.31	0	s_t
15	2.72 ± 0.04	16.3 ± 0.1	0.23 ± 0.01	0.81 ± 0.03	OSC	Max 0.33	0.40	29.0	22.7	−22	0.09	0.39	0	s_t
16	2.67 ± 0.07	17.5 ± 0.1	0.67 ± 0.05	0.30 ± 0.01	OSC	0.82	0.78	70.2	50.3	−28	0.63	0.71	1.99	8.17
17	2.67 ± 0.05	17.7 ± 0.1	1.15 ± 0.06	0.316 ± 0.007	OSC	Max 0.70	0.75	28.8	37.4	30	0.67	0.70	0	8.65
18	2.73 ± 0.04	16.7 ± 0.1	0.47 ± 0.02	0.65 ± 0.05	OSC	Max 0.58	0.60	28.5	28.7	1	0.25	0.49	0.88	s_t
19	2.74 ± 0.03	16.6 ± 0.1	0.27 ± 0.01	0.61 ± 0.05	OSC	0.46	0.59	38.6	35.3	−9	0.18	0.51	1.01	s_t
20	2.73 ± 0.02	16.7 ± 0.1	0.127 ± 0.009	0.835 ± 0.008	BF	NA	0.43	NA	Stable	NA	0	0.37	0	s_t

(SS1, SS2, SS3 and OSC) as well as other flow patterns such as slug (SF), plug (PF) and bubbly (BF) flow observed in the experiments. The identification of the different types of severe slugging was made visually and from the analysis of the pressure histories at the bottom of the riser. The slug length was estimated as the product of the mean liquid superficial velocity times the slug production time. It can be observed that, due to actuation of the control system, there were some fluctuations around the mean value of pressure at the separator. It can also be observed that the pressure oscillations at the pipeline interacted with the inlet flow systems, causing oscillations in the flowrate of air and water.

As a consequence of the severe slugging phenomenon, the fluctuations in the variables representing the boundary conditions and also because of the characteristic fluctuations of the intermittent flow, a distribution of frequencies appears in the experimental pressure history at the bottom of the riser. The determination of the period of severe slugging and the identification of the flow pattern can be made with the aid of the Fast Fourier Transform (FFT). The experimental periods appearing in Tables 3–5 were determined from the corresponding FFT of the pressure signal at the bottom of the riser, using the software MATLAB (Magrab et al., 2005).

As an example corresponding to an unstable condition, Fig. 17a shows the FFT corresponding to the pressure history at the bottom of the riser of Fig. 10. It can be observed that for the reported SS1, SS2 and SS3 configurations a dominant frequency appears, from which it is possible to determine a severe slugging period; these period could also be calculated as the mean value corresponding to many experimental limit cycles.

Fig. 17b shows the FFT corresponding to the pressure history at the bottom of the riser of Fig. 14. It can be observed that for the reported slug, plug or bubbly flow configurations the spectral

Table 5
Comparison with experimental results for P_s = 3 bar g (Wordsworth et al., 1998).

Case	Experiment								Simulation					
	P_s	T (°C)	j_{g0} (m/s)	j_{l0} (m/s)	Type	ΔP_{exp} (bar)	$\alpha_{p\,exp}$ (–)	T_{exp} (s)	T_{sim} (s)	Error (%)	ΔP_{sim} (bar)	$\alpha_{p\,sim}$ (–)	x_{max} (m)	$s_{u\,min}$ (m)
1	4.20 ± 0.04	35.3 ± 0.1	0.69 ± 0.01	0.594 ± 0.001	SF	NA	0.50	NA	Stable	NA	0	0.52	0	s_t
2	4.06 ± 0.04	48 ± 3	0.095 ± 0.009	0.133 ± 0.001	SS3	0.64	Max 0.80	96.8	100	3	0.15	0.84	1.08	12.46
3	4.09 ± 0.04	30.4 ± 0.2	0.14 ± 0.01	0.298 ± 0.001	SS3	Max 0.75	Max 0.70	70.0	53.9	−23	0.11	0.71	0.49	s_t
4	4.15 ± 0.02	50.4 ± 0.1	0.23 ± 0.01	0.133 ± 0.009	SS3	0.72	0.80	89.7	79.8	−11	0.28	0.84	1.17	11.39
5	4.15 ± 0.02	50.4 ± 0.1	0.23 ± 0.01	0.1323 ± 0.0009	SS3	0.71	0.80	90.6	79.8	−12	0.28	0.84	1.17	11.38
6	4.19 ± 0.07	38.0 ± 0.3	0.66 ± 0.03	0.302 ± 0.001	OSC	Max 0.81	0.65	31.3	37.5	20	0.35	0.71	0.56	12.28
7	4.02 ± 0.06	36.2 ± 0.2	0.26 ± 0.01	0.302 ± 0.001	OSC	Max 0.64	0.72	38.9	47.2	21	0.18	0.71	0.61	s_t
8	4.06 ± 0.07	31.4 ± 0.2	0.46 ± 0.02	0.3007 ± 0.0009	OSC	Max 0.74	0.74	34.7	43.3	25	0.29	0.71	0.84	12.50
9	4.15 ± 0.02	32.1 ± 0.1	0.083 ± 0.005	0.596 ± 0.001	OSC	Max 0.30	Max 0.53	34.4	Stable	NA	0	0.51	0	s_t
10	4.17 ± 0.05	50.4 ± 0.1	0.40 ± 0.01	0.1321 ± 0.0008	OSC	Max 0.51	0.78	42.4	67.0	58	0.40	0.84	0.57	10.24
11	4.17 ± 0.04	34.9 ± 0.2	0.43 ± 0.01	0.592 ± 0.001	OSC	Max 0.55	0.50	27.2	Stable	NA	0	0.52	0	s_t
12	4.13 ± 0.04	33.3 ± 0.6	0.26 ± 0.01	0.599 ± 0.002	OSC	Max 0.64	Max 0.59	30.7	Stable	NA	0	0.51	0	s_t
13	4.16 ± 0.05	34.7 ± 0.3	0.109 ± 0.003	0.829 ± 0.003	BF	NA	0.42	NA	Stable	NA	0	0.37	0	s_t

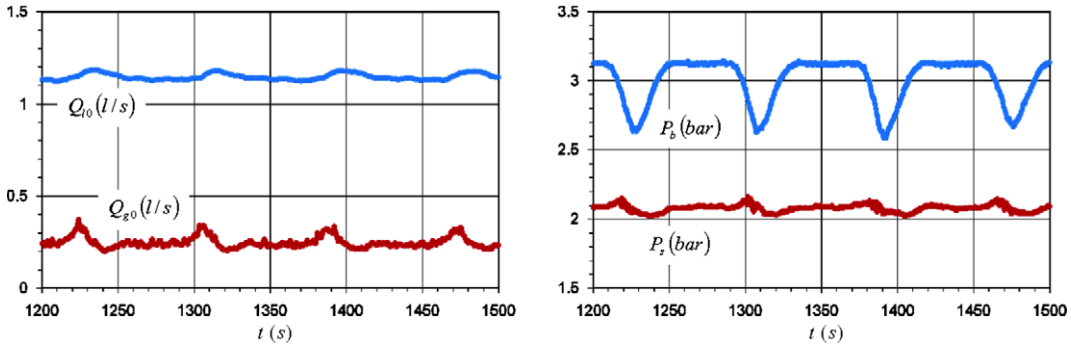

(a) Inlet flows. (b) Pressures.

Fig. 10. Experimental history for SS1 (case 2, Table 3).

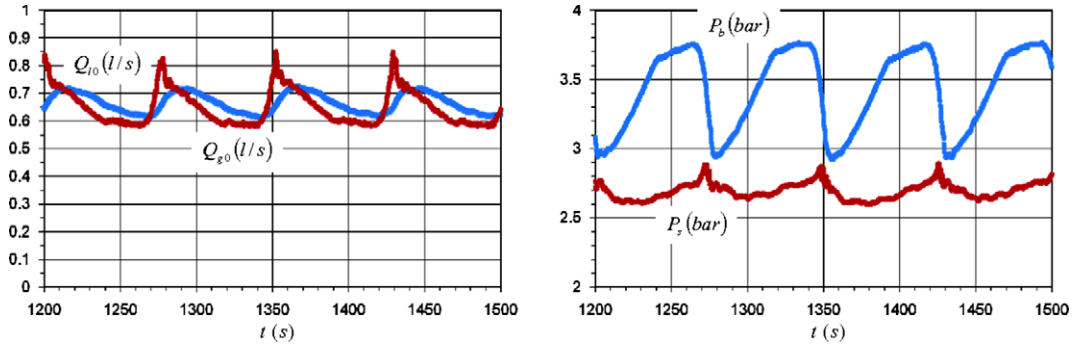

(a) Inlet flows. (b) Pressures.

Fig. 11. Experimental history for SS2 (case 7, Table 4).

components have low amplitudes and do not show a dominant frequency.

For the OSC configuration, the frequencies associated to severe slugging are near the ones associated to the natural flow intermittency and the amplitudes of the pressure cycles are smaller as the experimental configuration approaches the stability boundary. Although most of the pressure signals at the bottom of the riser for OSC configurations show FFT with a dominant peak, there are some in which two dominant peaks appear. As an example of this, in Fig. 18a and b are shown respectively the pressure signals and the FFT of pressure at the bottom of the riser; in this case, it can be observed some modulation.

7. Simulations

Necessary parameters were defined in order to simulate the experimental data corresponding to (Wordsworth et al., 1998) for a catenary riser, using air and water: $\mu_l = 1. \times 10^{-3}$ kg/m/s, $\mu_g = 1.8 \times 10^{-5}$ kg/m/s, $\rho_l = 1. \times 10^{3}$ kg/m^3, $R_g = 287$ m^2/s^2/K. Pipeline parameters are: $L = 57.4$ m, $L_e = 0$ m, $\beta = 2°$. Parameters for catenary riser are: $Z = 9.886$ m, $X = 6.435$ m, resulting from Eq. (46) $s_t = 12.5463$ m. Common parameters for pipeline and riser are: $D = 5.25018 \times 10^{-2}$ m, $\epsilon = 4.6 \times 10^{-5}$ m.

After the convergence study of Section 5, the riser was discretized with $N = 51$ nodes and simulations were performed for each

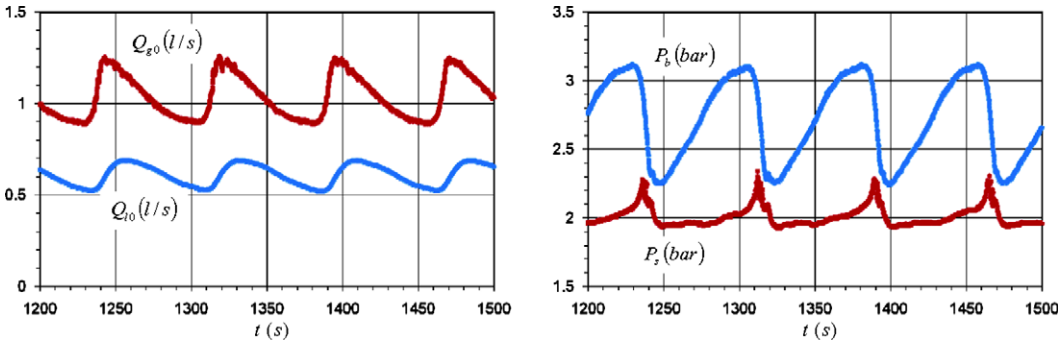

(a) Inlet flows. (b) Pressures.

Fig. 12. Experimental history for SS3 (case 11, Table 3).

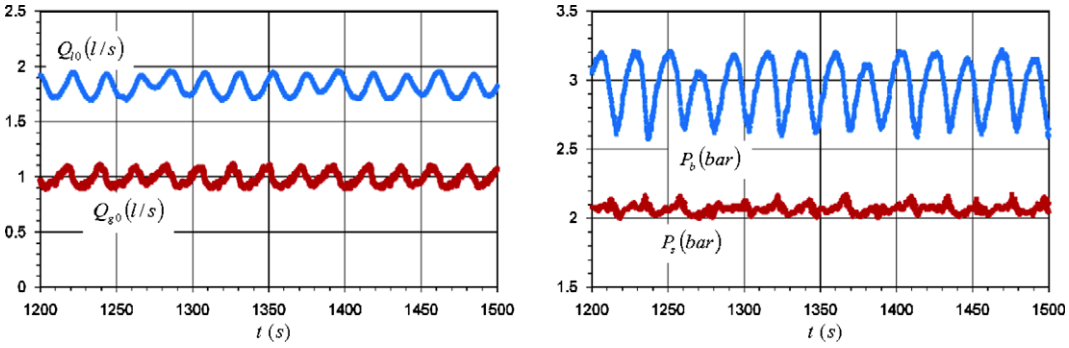

(a) Inlet flows. (b) Pressures.

Fig. 13. Experimental history for OSC (case 17, Table 3).

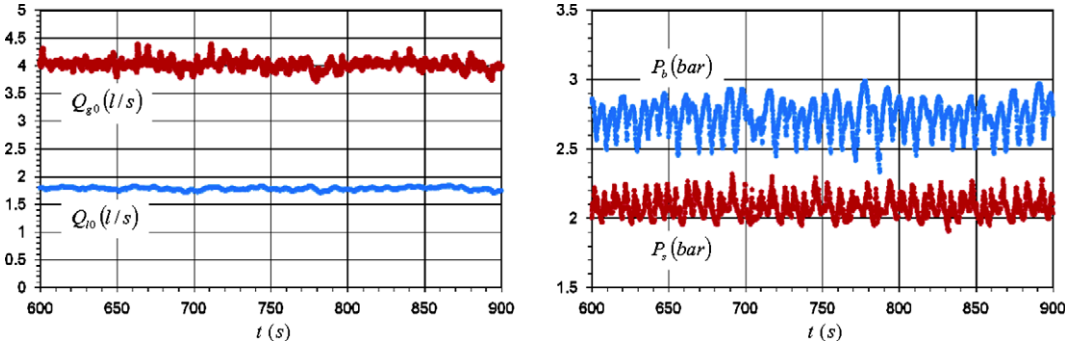

(a) Inlet flows. (b) Pressures.

Fig. 14. Experimental history for slug flow (case 14, Table 3).

experimental run, using the mean values. As an example, simulation results are shown for case 2, Table 3, corresponding to the following boundary conditions: $P_s = 2.08$ bar a, $Q_{l0} = 1.14 \times 10^{-3}$ m^3/s and $\dot{m}_{g0} = 2.9 \times 10^{-4} kg/s$.

The following results were obtained for variables at representative locations at the stationary state: $P_b = P_g = 3.02$ bar a, $\alpha_p = 0.558$, $\alpha_b = 0.0381$, $j_{g\ b} = 0.0373$ m/s, $j_{l\ b} = 0.526$ m/s, $x = 0$ m, $s_u = s_t$, $\alpha_u = 0.0526$, $j_{gu} = 0.0541$ m/s, $j_{lu} = 0.526$ m/s. The void fraction at the pipeline from the stationary state is shown in Tables 3–5 as $\alpha_{p\,sim}$.

Setting the stationary solution as initial condition for the transient program, it was observed that the system destabilizes and reaches a limit cycle. For this case, a simulation time of 1000 s was chosen, in order to let the system reach a cyclic response.

In Fig. 19 it is shown the limit cycle simulation corresponding to the pressure at the bottom of the riser. From this figures it is possible to determine the simulated cycle period, resulting $T_{sim} = 80.4$ s.

The following figures show the limit cycles simulations corresponding to different variables necessary to characterize the type of severe slugging: void fraction at the bottom of the riser (Fig. 20a), void fraction at the liquid level in the riser (Fig. 20b), gas superficial velocity (Fig. 20c) and liquid superficial velocity (Fig. 20d) at the bottom of the riser, gas superficial velocity (Fig. 20e) and liquid superficial velocity (Fig. 20f) at the liquid level

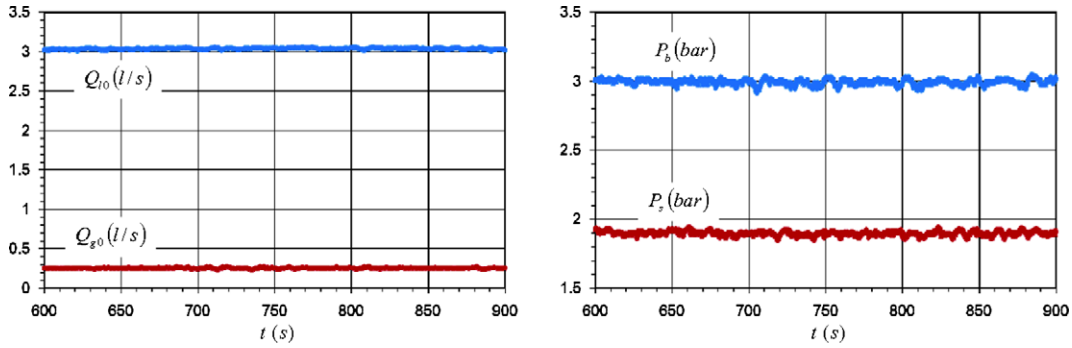

(a) Inlet flows. (b) Pressures.

Fig. 15. Experimental history for plug flow (case 16, Table 3).

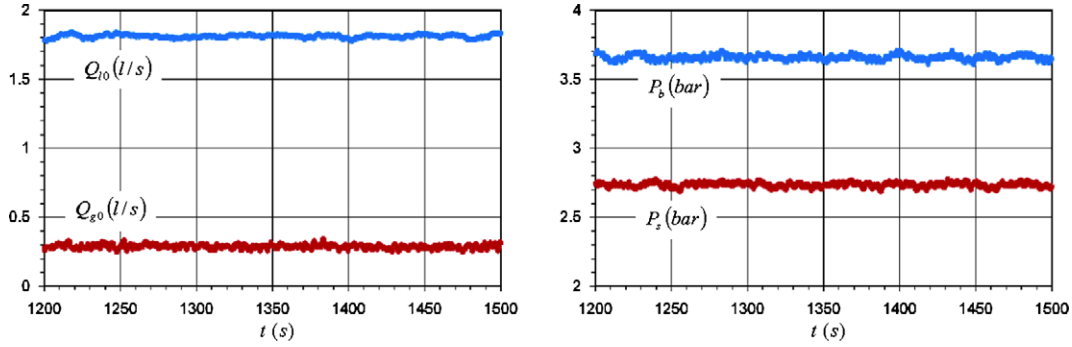

(a) Inlet flows. (b) Pressures.

Fig. 16. Experimental history for bubbly flow (case 20, Table 4).

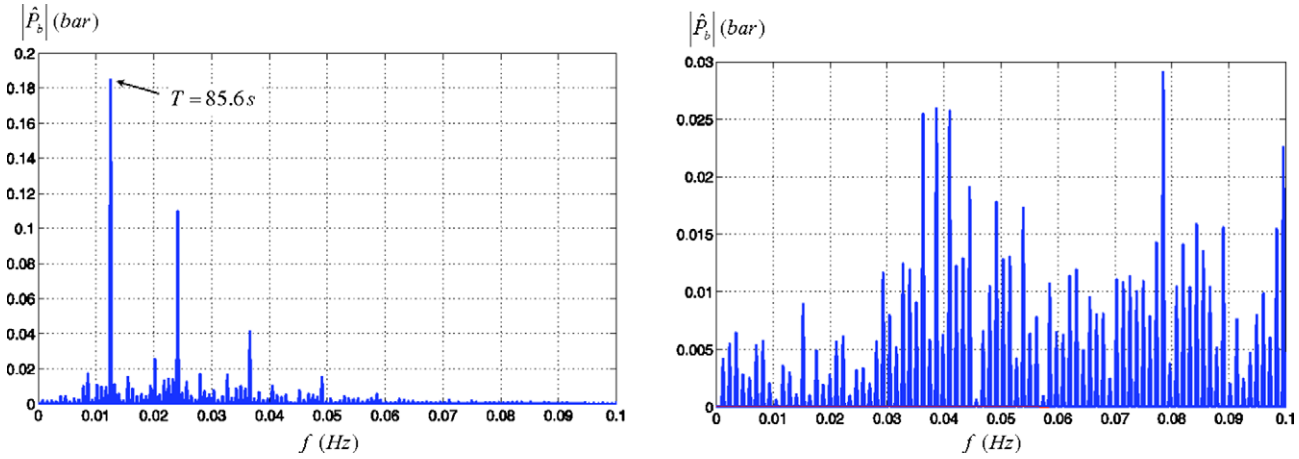

(a) SS1 (case 2, Table 3). (b) Slug flow (case 14, Table 3).

Fig. 17. FFT for different pressures histories.

in the riser, position of liquid accumulation front (Fig. 20g) and position of liquid level at the riser (Fig. 20h).

Many parameters corresponding to the transient can be calculated from Fig. 20a to h. Considering that the slugging cycle begins when the gas passage at the bottom of the riser is blocked, times corresponding to different stages described in Section 1 can be calculated, such as the slug formation time (14.3 s), slug production time (47.3 s), bubble penetration time (10.5 s) and gas blowdown time (8.3 s). The slug length can be calculated by integrating the liquid superficial velocity at the top of the riser in the period in which the void fraction is zero, resulting $L_s = 33.4$ m; as $L_s > s_t$, this transient characterizes a severe slugging type 1 (Wordsworth et al., 1998). In this case, the liquid level remains at the top of the riser.

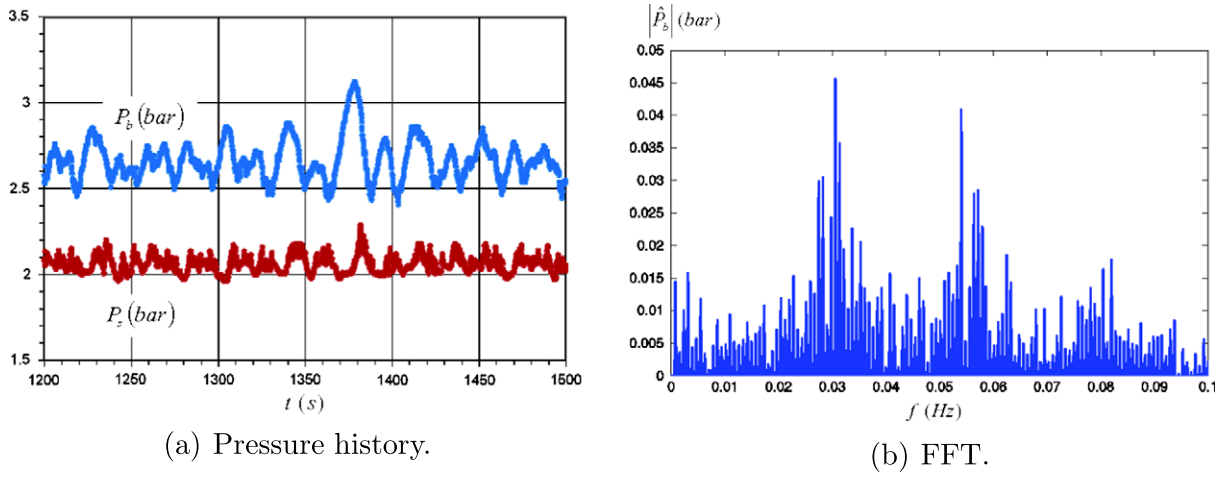

(a) Pressure history. (b) FFT.

Fig. 18. Pressure history and FFT for case 13, Table 3.

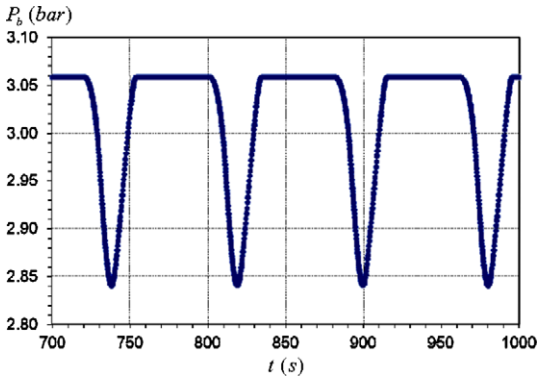

Fig. 19. Simulated limit cycle, pressure at the bottom of the riser (type SS1, case 2, Table 3).

From the simulations, it is possible to determine the severe slugging periods T_{sim}, the pressure amplitude at the bottom of the riser ΔP_{sim}, the maximum position of the liquid penetration front in the pipeline x_{max} and the minimum position of the liquid level in the riser $s_{u\,min}$, which are shown in Tables 3–5. The periods calculated with the model are in very good agreement with the experimental ones. There are some points in which the error is high; in these experimental points it was not possible to keep constant low values for the volumetric flowrates; an example of this is shown in Fig. 21 for case 4, Table 3.

The simulations were convergent for different time steps and did not show the problem of "infinite gas penetration" at the bottom of the riser (Taitel et al., 1990; Sarica and Shoham, 1991). As a consequence, the program can also be used to predict the flow regime maps within the unstable region.

8. Stability and flow regime maps

Fig. 22 shows the stability map corresponding to the separator pressure P_s = 2.013 bar a and temperature T = 20 °C, representative values for the data corresponding to Table 3. The numeric stability curve was obtained by keeping constant a value of liquid or gas flow rate and varying the other in fixed increments until passing from one condition (stable or unstable) to another; when this happens, the procedure is repeated with half the increment until achieving convergence. The procedure is laborious and computationally costly. In the same figure the experimental data corresponding to Table 3 are shown. An excellent agreement is observed in the prediction of the stability region for the different reported types of severe slugging.

Figs. 23 and 24 show the experimental data corresponding to Table 4 and 5, as well as the stability curves built using representative values (P_s = 2.70 bar a and T = 20 °C for Fig. 23, P_s = 4.10 bar a and T = 40 °C for Fig. 24). It can be observed that the compression of the gas phase has a stabilizing effect, reducing the region of unstable flow. The compression stabilizing effect can be also achieved through the closure of a choking valve at the top of the riser. These trends were reported in (Taitel, 1986).

It is worth noting that, in the model, it is possible to identify SS types 1, 2 and 3 but slug, plug and bubbly flows are regarded as stable; moreover, the model cannot distinguish between SS3 and OSC (both flow patterns are unstable, with continuous gas penetration at the bottom of the riser). Fig. 25 shows the numerically built flow regime map corresponding to the types of severe slugging defined above for P_s = 2.013 bar a and T = 20 °C. The boundaries between SS1–SS2 and SS2–SS3 were obtained with a similar procedure as the one used for the stability curve. For the boundary SS1–SS2 there were detected the points in which the $L_s = s_t$, while for the boundary SS2–SS3 there were detected the points in which $j_{g\,b} = 0$. Although there are some discrepancies in the location of the boundaries when compared to the experimental data, it can be observed a qualitatively good description of the different regions.

An interesting result coming from the flow regime map is that the SS3 region extends within a range of gas flows in the unstable region, for small liquid flows. As oscillations have relatively small amplitudes and periods for SS3, this means that a real system could operate in the unstable region, with acceptable pressure and flow fluctuations, depending on the geometry and characteristics of the separator. Moreover, near the stability curve it can be possible that a unstable experimental point be considered as stable if only a visual criterium is used to determine the type of severe slugging. It can also be observed that the region corresponding to SS2 is relatively narrow.

9. Conclusions

A dynamic model for severe slugging, applicable to risers with locally variable inclination angles, was developed. This model allows to identify the different types of severe slugging reported in literature, through the tracking of the liquid level in the riser and the liquid accumulation length at the pipeline. It is important to

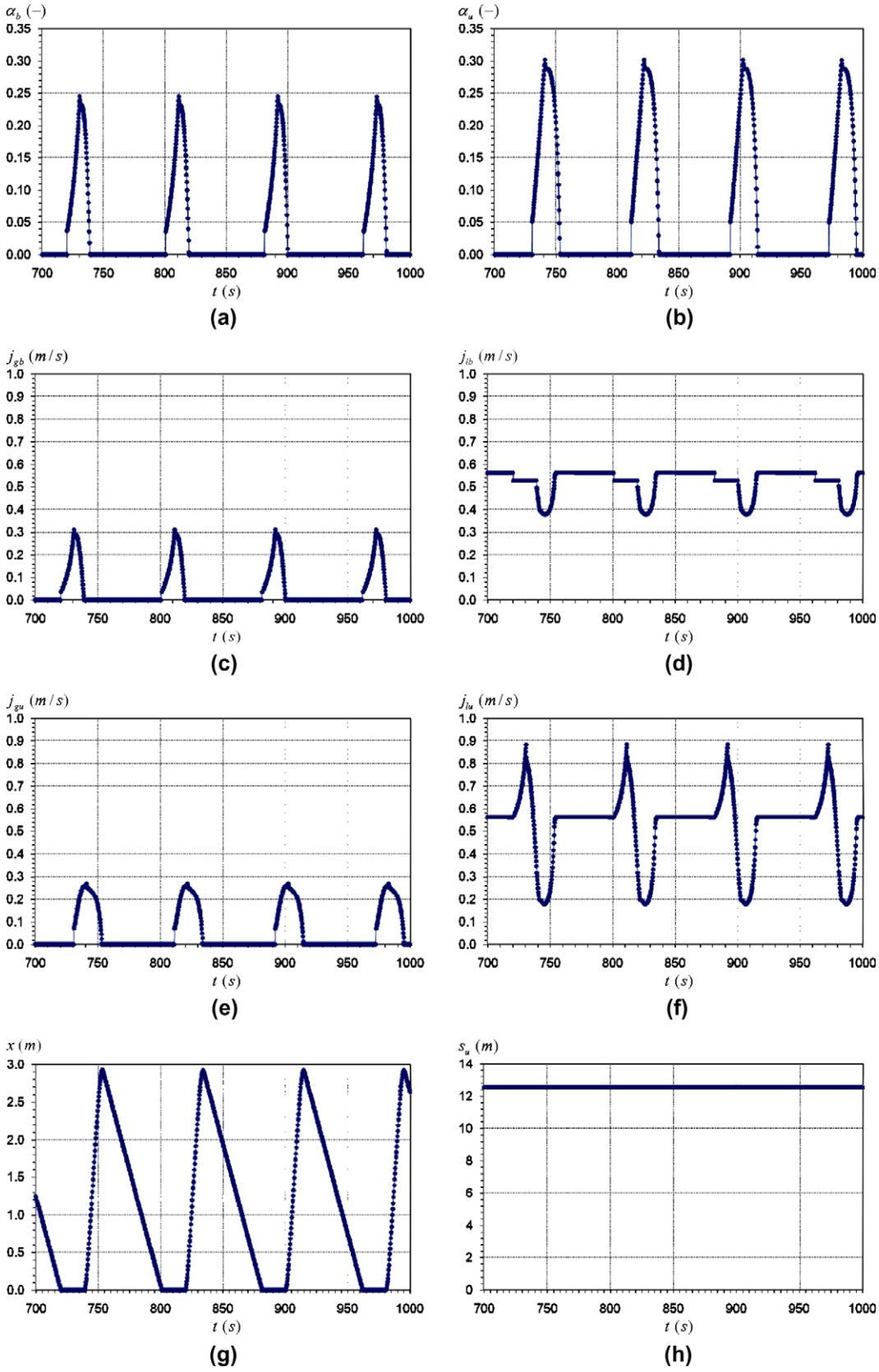

Fig. 20. Simulated limit cycles (type SS1, case 2, Table 3).

notice that the model does not have adjusted parameters from severe slugging experimental data.

The simulations were convergent for different time nodalizations and did not show the problem of "infinite gas penetration"

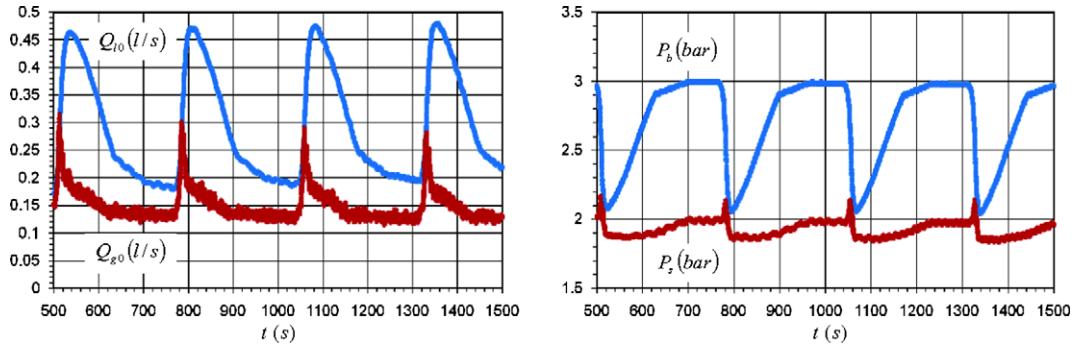

(a) Inlet flows. (b) Pressures.

Fig. 21. Experimental history for case 4, Table 3.

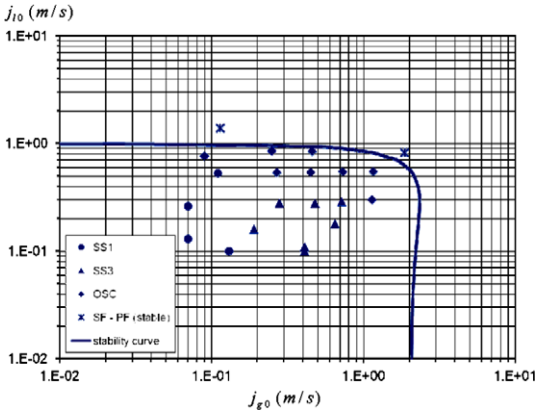

Fig. 22. Experimental data (Table 3) and stability map for $P_s = 2.013$ bar a and $T = 20$ °C.

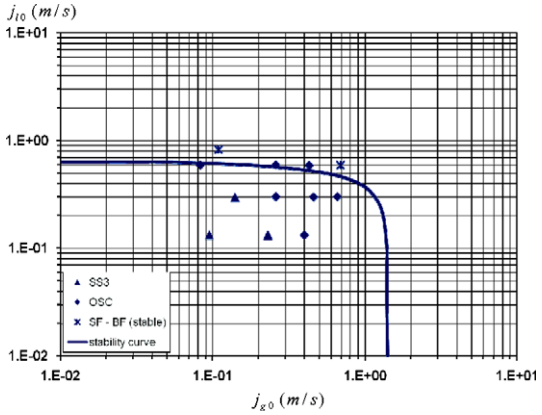

Fig. 24. Experimental data (Table 5) and stability map for $P_s = 4.10$ bar a and $T = 40$ °C.

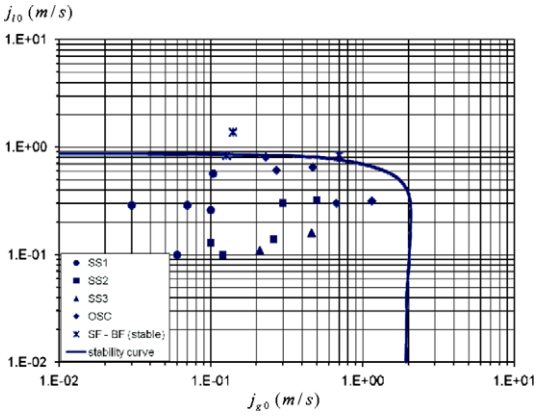

Fig. 23. Experimental data (Table 4) and stability map for $P_s = 2.70$ bar a and $T = 20$ °C.

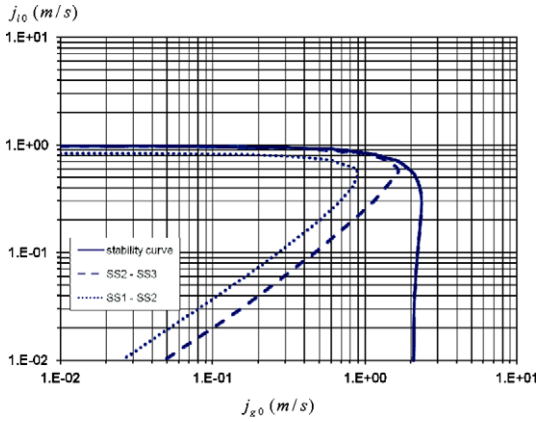

Fig. 25. Stability and flow regime map for $P_s = 2.013$ bar a and $T = 20$ °C.

at the bottom of the riser. As a consequence, the program can be also used to build stability and flow regime maps for different sets of system parameters.

The model was used to simulate the data from (Wordsworth et al., 1998) for a catenary riser. The results show a very good agreement between numerical and experimental severe slugging cycles, excellent prediction of the stability curve and a qualitatively good description of the flow regime curves.

Based on the obtained results, we conclude that the model presented in this paper captures well the main phenomena in multiphase flow in pipeline–riser systems. As future work, the linear stability analysis of the present model will be performed in order to obtain a more systematic procedure to generate stability maps in the system parameter space.

Acknowledgements

This work was supported by *Petróleo Brasileiro S. A.* (Petrobras). The authors wish to thank *Fundação de Amparo à Pesquisa do Estado*

de São Paulo (FAPESP, Brazil) and *Conselho Nacional de Desenvolvimento Científico e Tecnológico* (CNPq, Brazil).

References

Baliño, J.L., 2008. Análise de intermitência severa em risers de geometria catenária, Tese de Livre Docência em Engenharia (in Portuguese). Escola Politécnica, Universidade de São Paulo, p. 141.

Bendiksen, K.H., 1984. An experimental investigation of the motion of long bubbles in inclined tubes. Int. J. Multiphase Flow 10, 467–483.

Bœ, A., 1981. Severe slugging characteristics. Part I: Flow regime for severe slugging. Part II: Point model simulation study. Selected Topics in Two-Phase Flow. Trondheim, Norway.

Burr, K.P., Baliño, J.L., 2007. Assymptotic solution for the stationary state of two-phase flows in pipeline–riser systems. In: XIX International Congress of Mechanical Engineering (COBEM 2007), Brasilia, Brazil, p. 10.

Chen, N.H., 1979. An explicit equation for friction factor in pipe. Ind. Eng. Chem. Fundam. 18, 296–297.

Chexal, B., Lellouche, G., Horrowitz, J., Healzer, J., 1992. A void fraction correlation for generalized applications. Progress in Nuclear Energy 27, 255–295.

Drew, D.A., Passman, S.L., 1999. Theory of Multicomponent Fluids. Springer-Verlag, New York, ISBN 0-387-98380-5.

Jansen, F.E., 1990. Elimination of severe slugging in a pipeline–riser system. M.S. Thesis, The University of Tulsa.

Kokal, S.L., Stanislav, J.F., 1989. An experimental study of two-phase flow in slightly inclined pipes – I. Flow patterns. Chem. Eng. Sci. 44, 665–679.

Magrab, E.B., Azarm, S., Belachandran, B., Duncan, J.H., Herold, K.H., Walsh, G.C., 2005. An Engineer 's Guide to MATLAB, second ed. Pearson Prentice Hall, ISBN 0-13-145499-4.

Masella, J.M., Tran, Q.H., Ferre, D., Pauchon, C., 1998. Transient simulation of two-phase flows in pipes. Int. J. Multiphase Flow 24, 739–755.

Mokhatab, S., 2007. Severe slugging in a catenary-shaped riser: experimental and simulation studies. Pet. Sci. Technol. 25, 719–740.

Sarica, C., Shoham, O., 1991. A simplified transient model for pipeline–riser systems. Chem. Eng. Sci. 46, 2167–2179.

Schmidt, Z., 1997. Experimental study of two-phase slug flow in a pipeline–riser system. Ph.D. Dissertation, The University of Tulsa.

Taitel, Y., 1986. Stability of severe slugging. Int. J. Multiphase Flow 12, 203–217.

Taitel, Y., Dukler, A.E., 1976. A model for predicting flow regime transitions in horizontal and near horizontal gás–liquid flow. AIChE J. 22, 47–55.

Taitel, Y., Vierkand, S., Shoham, O., Brill, J.P., 1990. Severe slugging in a riser system, experiments and modeling. Int. J. Multiphase Flow 16, 57–68.

Tannehill, J.C., Anderson, D.A., Pletcher, R.H., 1997. Computational Fluid Mechanics and Heat Transfer. Taylor & Francis, ISBN 1-56032-046-X.

Vierkandt, S., 1998. Severe slugging in a pipeline–riser system, experiments and modelling. M.S. Thesis, The University of Tulsa.

Wordsworth, C., Das, I., Loh, W.L., McNulty, G., Lima, P.C., Barbuto, F., 1998. Multiphase Flow Behaviour in a Catenary Shaped Riser, vol. I, II & III, CALtec Report No.: CR 6820.